THE CRUSTAL STRUCTURE OF THE MARMARA REGION USING RECEIVER FUNCTION ANALYSIS

by

Pınar BÜYÜKAKPINAR

B.S, Geophysics Engineering, Süleyman Demirel University, 2009

Submitted to the Institute for Graduate Studies in
Science and Engineering in partial fulfillment of
the requirements for the degree of
Master of Science

Graduate Program in Geophysics

Boğaziçi University

2013

THE CRUSTAL STRUCTURE OF THE MARMARA REGION USING RECEIVER FUNCTION ANALYSIS

APPROVED by:

Prof. Dr. Cemil GÜRBÜZ (Thesis Supervisor)	……
Prof. Dr. Ali PINAR	……
Prof. Dr. Gündüz HORASAN	……
Assoc. Prof. Ekrem ZOR (Thesis Co-Supervisor)	……
Assit. Prof. Özgün Konca	……

DATE OF APPROVAL: 26.08.2013

TABLE OF CONTENTS

ACKNOWLEDGEMENTS

First of all, I would like to express my sincere appreciation and gratitude to my advisor, Prof. Dr. Cemil Gürbüz, for his enlightening guidance and inspiring instruction in the development and completion of this study. He always gave me useful suggestions so that I could improve my research and wiriting skills.

I would like to give special thank to my co-supervisor, Assoc. Prof. Ekrem Zor, for his guidance, insight, endeavor, and support throughout this research as well as providing me computer programs to enhance my study during the data processing stages.

In addition, I would like to thank Doğan Kalafat and Mehmet Yılmazer from UDIM who provided me the data which is necesssary for my study. I would also like to thank Onur Tan from TUBITAK for sharing the data set.

My greatest appreciation and friendship goes to my closest friend and officemate, Esra Kalkan, who always make me smile and listen to me in difficult and happy moments of my life. I appreciate her support, our relaxing moments and the nice time we shared together. Many thanks to Sezim Ezgi Işık who helped me with a smile upon her face whenever I was in trouble especially in computer programs. I would also like to thank all of my friends and members of Kandilli Observatory and Earthquake Research Institute for encouraging me to continue on and finish up my thesis. My research would not have been possible without their helps.

Finally, I would like to thank my wonderful family for their unconditional love and support. My mother and father deserve special recognition for being the best role models I could imagine. My brother has been my best friend all my life and I love him dearly and thank him for all his advice and support.

ABSTRACT

THE CRUSTAL STRUCTURE OF THE MARMARA REGION USING RECEIVER FUNCTION ANALYSIS

The Marmara Region is a rapidly deforming area with high seismic activity in the northwestern Turkey. In order to further understand the crustal structure in the region, we present results from receiver function analysis using the permanent stations in the region by applying H-κ stacking algorithm which gives crustal thickness and Vp/Vs ratio beneath a station. 40 land stations between January of 2008 and April of 2012, and five cabled Sea Bottom Observatories which were deployed at the end of 2010 by Kandilli Observatory and Earthquake Research Institue located between 40.2°-41.2° N and 26.5°-30.5° E were included in the analysis. Approximately 250 teleseismic events from a wide range of epicentral distances with magnitudes greater than Mw 5.5 are used to obtain receiver functions. Furthermore, in order to calculate the receiver functions in time domain using iterative deconvolution technique suggested by Ligorria and Ammon (1999). Consequently, the crustal structure of the region has been reasonably defined and compared with the other studies. As a consequence of the receiver function analysis, the Moho depth variation map and Vp/Vs ratio map were plotted. The Moho depth on average is 31 km. There are no sharp changes in the crustal thickness of the Marmara Region except North Marmara Trough because basin structure of the Marmara Sea where crustal thickness reaches up to 26 km in the same region was not observed. Furthermore, we found overall average Vp/Vs ratio of 1.74, for the region but we obtained low Vp/Vs ratios in the stations located near Çınarcık Basin which varies between 1.64 - 1.74 indicating the effect of basin structure in the area and North Marmara where Vp/Vs ratios vary between 1.60 and 1.70 whichis related to the sediment structure of the area. We also acquired higher Vp/Vs ratios which are between 1.86 and 1.96 in the Western Marmara Region. This can be due to increasing mafic content in this area. Additionally, an attempt has been made to invert the radial receiver function of the station KCTX using iterative linear 1D inversion method in order to compare the Moho depth values with two different techniques.

ÖZET

ALICI FONKSİYONLARI KULLANARAK HESAPLANAN MARMARA BÖLGESİ KABUK YAPISI

Marmara Bölgesi, Türkiye'nin kuzey batısında yer alan yüksek sismik aktivite ile hızlı deforme olmuş bir bölgedir. Bölgedeki kabuk yapısını daha iyi anlamak için; bölgedeki kalıcı deprem istasyonları kullanılarak, alıcı fonksiyonu analizlerinden bir istasyon altındaki kabuk kalınlığını ve Vp/Vs oranını veren H-κ yığma algoritmasını uygulayarak sonuçlar alınmıştır. 2008 Haziran ve 2012 Nisan tarihleri arasında, 40.2°-41.2° B ve 26.5°-30.5° E arasında kalan bölgede bulunan 40 adet kara istasyonu ve 2010 yılının sonunda KOERI tarafından yerleştirilen beş adet denizaltı gözlemcisi bu çalışmaya dahil edilmiştir. Alıcı fonksiyonları elde etmek için, geniş bir merkez üssü uzaklık aralığında, Mw değeri 5.5 ve üzeri olan yaklaşık 250 uzak deprem kullanıldı. Ayrıca, zaman ortamında alıcı fonksiyonları hesaplamak için, Ligorria and Ammon (1999) tarafından ortaya atılan Tekrarlamalı Ters Evrişim Tekniği kullanıldı. Sonuç olarak, bölge için makul bir kabuk yapısı belirlendi ve diğer çalışmalarla karşılaştırıldı. Alıcı fonksiyonu analizleri sonunda, Moho derinliğinin ve Vp/Vs oranının değişimini gösteren haritalar çizildi. Marmara Denizi'nin basen özelliği gösteren ve kabuk kalınlığı 26 km'ye kadar uzanan Kuzey Marmara alt basen bölgesi hariç, kabuk kalınlığında ani keskin değişimler gözlemlenmedi ve Moho derinliği ortalama olarak 31 km hesaplandı. Buna ek olarak, ortalama Vp/Vs oranı 1.74 olarak bulundu. Çınarcık Havzası yakınlarındaki istasyonlarda, 1.60-1.74 arasında değişen düşük Vp/Vs oranları ve Kuzey Marmara'da 1.60-1.70 arasında değişen ve bölgenin sediman yapısına karşılık gelen düşük Vp/Vs oranları gözlemlendi. Diğer taraftan, mafik içeriği fazla olan Batı Marmara Bölgesi'nde, 1.86-1.96 arasında değişen Vp/Vs oranları elde edildi. Bunların yanısıra, KCTX istasyonun radyal alıcı fonksiyonunu ters çözümlemek için yinelemeli doğrusal bir boyutlu ters çözüm yöntemi kullanarak, Moho derinliği farklı iki yöntemle karşılaştırılmış oldu.

LIST OF FIGURES

LIST OF TABLES

LIST OF SYMBOLS

1D	One Dimensional
2D	Two Dimensional
3D	Three Dimensional
BAZ	Backazimuth
EW	East-West
H	Thickness
κ	Vp/Vs
MSC	Multi Channel Seismic
Mw	Moment Magnitud
NAF	North Anatolian Fault
NAFZ	North Anatolian Fault Zone
NS	North-South
NW	North-West
OBS	Ocean Bottom Seismometer
RF	Receiver Function
RT	Radial-Transverse
RTZ	Radial-Transverse-Vertical
SW	South-West
Vp	P wave velocity
Vs	S wave velocity
WARR	Wide Angle Reflection Refraction

1. INTRODUCTION

For the sake of simplicity, the interior of the earth can be assumed to have horizontal layers affecting the seismic energy arriving at a given station.Using this assumption, obtaining the seismic velocities of the horizontally layered earth model is relatively easy by using seismic wave recordings that are created by natural or artificial sources. In this point of view, the first attempt to investigate the boundary between the Earth's crust and the mantle was made by Mohorovicic (1909). The boundary is named as Moho discontunity when he found an increase of velocity beneath the shallow rocks in Europe.

The knowledge of the Moho depth may be used to understand the type of crust, the structure of crust and the tectonic evolution of continents. For this purpose, teleseismic body waves have been used extensively for a long time to reveal crustal and lithospheric structures beneath recording stations. Phinney (1964) used spectral amplitude ratio of the three component recordings under the name of crustal transfer method. The method has been subsequently improved by Burdick and Langston (1977). Langston (1979) finally developed receiver function method by using time domain transformation of the complex spectral ratio of the three component recordings. Later, Owens *et al.,* (1984) applied linearized time-domain inversion routine to the receiver function obtained from broad-band data. Several authors are then addressed the issue of non-uniqueness of the receiver function inversion with different inversion algorithms (Ammon *et al.,* 1990; Özalaybey *et al.,* 1997; Sandvol *et al.,* 1999; Sambridge *et al.,* 1999). It is now one of the most widely used technique to determine the crustalstructure beneath the seismic stations.

Various studies have been done in order to better understand the tectonic evolution of Marmara Region especially after the 17th August 1999 İzmit earthquake which caused extensive damage and high loss of human life. However, the studies comprise mainly eastern part of the Marmara Region. Therefore, we wanted to apply the receiver function method for the whole Marmara Region to determine the depth to Moho discontinuity and Vp/Vs ratio. The waveforms of approximately 250 teleseismic events extracted from the continuoes recordings of the 40 land and five cabled Sea Bottom Observatory Stations for

a wide range of epicentral distances with magnitudes greater than Mw 5.5 were used to obtain receiver functions to better understand the variation of Moho depth and Vp/Vs ratios in the Marmara Region.

In order to analyze the teleseismic data, we applied usual processes such as rotating three component records to obtain radial and transverse components and filtering to suppress noise and also remove the effect of small-scale heterogenities. After these steps, we computed the receiver functions in the time domain using the iterative deconvolution technique suggested by Ligorria and Ammon (1999). Finally, we applied H-κ stacking analysis method which is a transformation from the time domain of receiver function directly into H (depth) and the Vp/Vs ratio. The H-κ stacking method has been used by several scientists (e.g. Zhu and Kanamori, 2000; Julia *et al.*, 2005; Julia and Mejia, 2004) recently.

In this thesis, we presented brief information about the geology and tectonics of the region in the 2nd Chapter. In the 3rd Chapter, we gave the methodology of H-κstacking algorithm and receiver function technique in details. In the 4rd Chapter we presented the data set and station distrubiton. Finally, we showed the H-κ stacking map for each station and discussed the results with the Moho depth and Vp/Vs variation map in the 5th Chapter.

2. TECTONICS OF THE MARMARA REGION AND PREVIOUS STUDIES

2.1. Tectonics of the Marmara Region

The Marmara Region is located in northwest Turkey and it is situated between the Aegean, Balkan, Black Sea, and Anatolian regions. The region is a transition zone between the strike slip regime of the North Anatolian Fault and the NS extension of the Aegean Sea Area. The area has witnessed several major historical earthquakes as shown in Figure 2.1. The most recent one, 17 August, 1999 İzmit earthquake (Mw=7.4) caused extensive damage and high loss of human life.

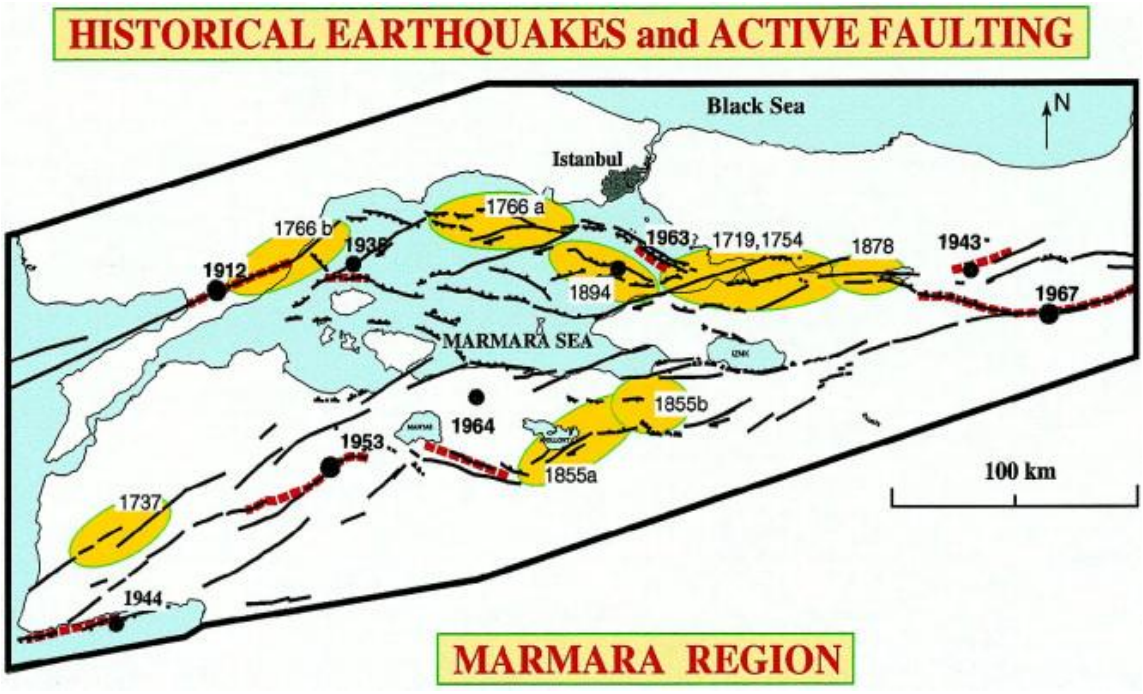

Figure 2.1. Active faulting and historical earthquakes in the Marmara Region (modified after Barka, 1997).

The NAF is a one of the largest plate bounding transform and well known seismically active strike slip fault that extends for about 1200 km from Karlıova Junction to mainland Greece between Eurasian, Anatolian Plates as shown in Figure 2.2. Anatolian plate, caught between the converging Eurasian and Arabian Plates, escapes westwards

along the dextral North Anatolian and sinistral East Anatolian faults into the NS extending Aegean (McKenzie, 1972). Current right-lateral slip rate is 20-30 mm/year (McClusky *et al.*, 2000). In the Marmara region, the NAF shows two features not observed in the rest of its 1200 km long fault zone (Okay *et al.*, 2000). There are several deep marine strike slip basins which are Çınarcık Basin, Central Basin, and Tekirdağ Basin from west to east constituting part of the Marmara Sea, and many NW and SW trending major dextral strike slip fault zones on land with no apparent relation to the west trending active branch of the NAF. Tectonic map of the Marmara Region represented in Figure 2.3.

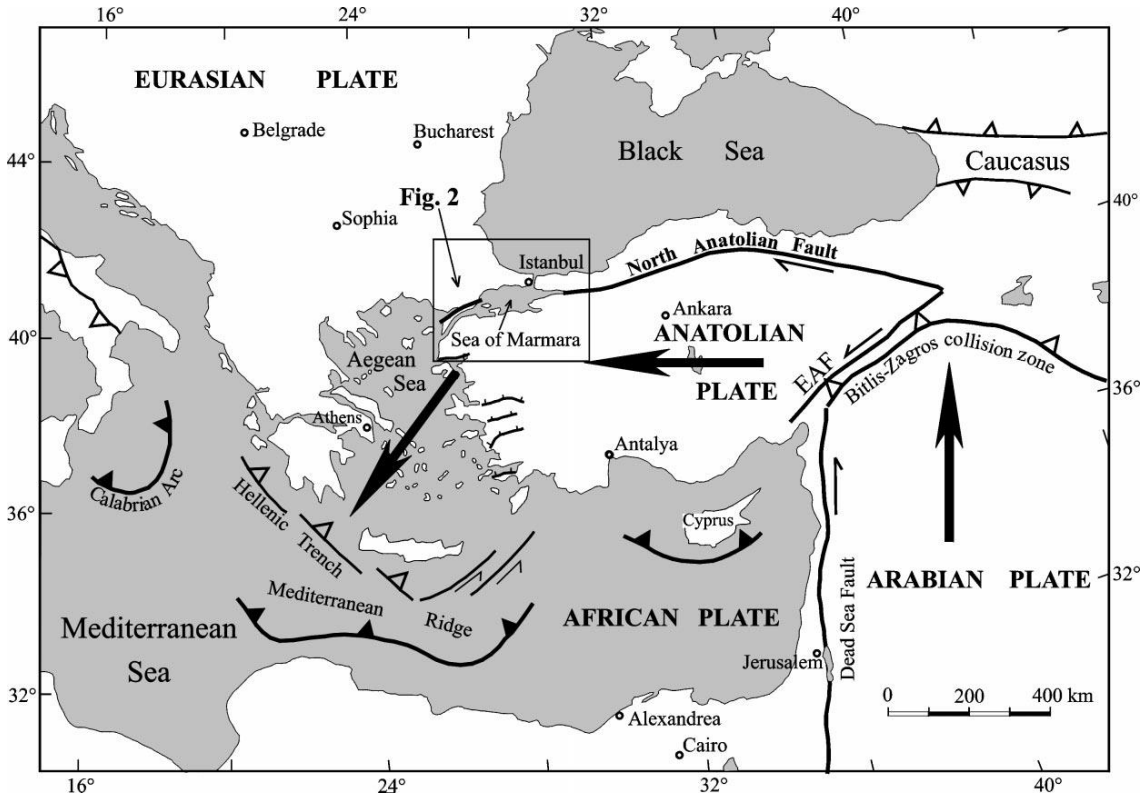

Figure 2.2. Active tectonic map of the Turkey and the rectangular area shows the Marmara Region. Lines with filled triangles show active subduction zones, lines with open triangles are active thrust faults at continental collision zones, and lines with tick marks are normal faults. The large solid arrows indicate the sense of motion of the lithospheric plates. EAF: East Anatolian Fault (Okay *et al.*, 2000).

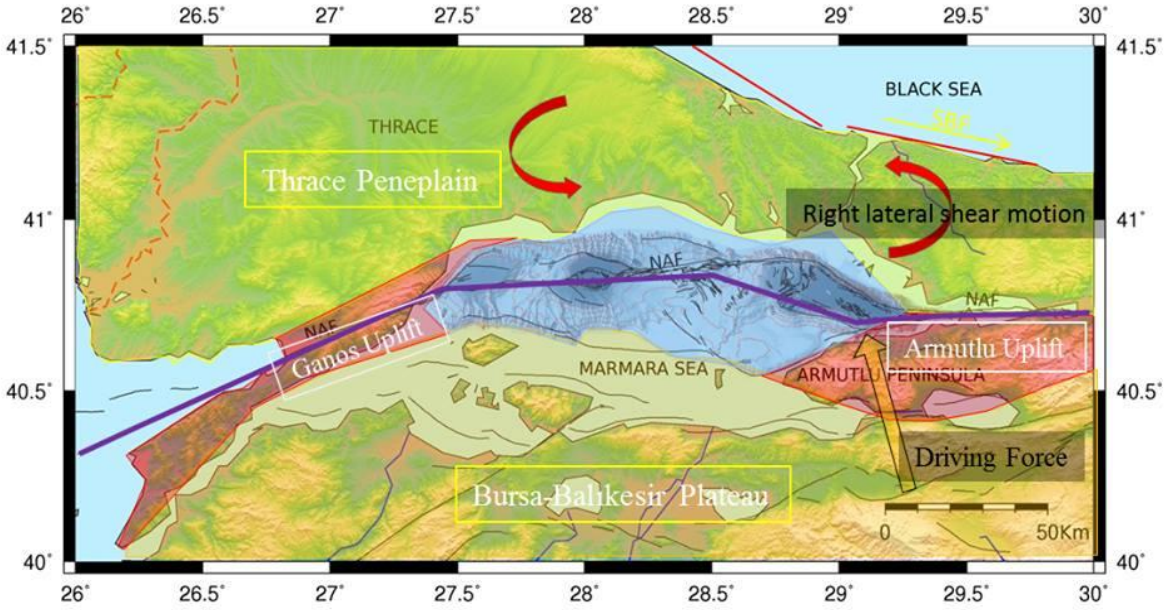

Figure 2.3. Tectonic map of the Marmara Region, red arrows shows the dextral shear stress in the region caused by two right lateral strike slip faults. (Y. Yılmaz, lecture notes, İTÜ, 2013, edited by Işık, 2013).

2.2. The Geology of the Marmara Region

Geologically, the Marmara Region consists of three terranes with different stratigraphies and tectonic histories. These are the Sakarya Zone to the south, the Istanbul Zone to the northeast and the Strandja Rhodopian terrane which crops out all along the northern, western and southern margins of the Thrace Basin (Figure 2.4.).

The İstanbul Zone is made of Precambrian crystalline basement extends along by a continuous transgressive sedimentary succession which ranges from Ordovician to Carboniferous which was deformed during the Hercynian Orogeny (Dean *et al.*, 1997; Görür *et al.*, 1997). Senonian andesites and small acidic intrusions widely exist (Okay and Tüysüz, 1999).

Figure 2.4. General geological structure of the Marmara Region and its surrounding areas (Okay, 2008).

The Sakarya Zone characterised by a Triassic subduction accretion complex which is called Karakaya Complex and consisted of strongly deformed and partly metamorphosed basement. The final phase of deformation occurred during the latest Triassic and was followed by sedimentation of Jurassic continental to shallow-marine deposits, Cretaceous carbonates, and finally by Senonian andesites (Altıner *et al.*, 1991; Tüysüz, 1993).

The Strandja Zone constitutes the easternmost part of the crystalline basement that includes metamorphic rocks interrupted by Permian Granites (Aydın, 1974; Okay and Tüysüz, 1999). Basement and Triassic succession were regionally metamorphosed during the mid-Jurassic and then overlain by Cenomanian conglomerates and shallow marine limestones. These are covered by Senonian andesites and intruded by associated granodiorites as in the case of the İstanbul Zone (Moore *et al.*, 1980). Geologic units of Western and Eastern Marmara Region was displayed in Figure 2.5.

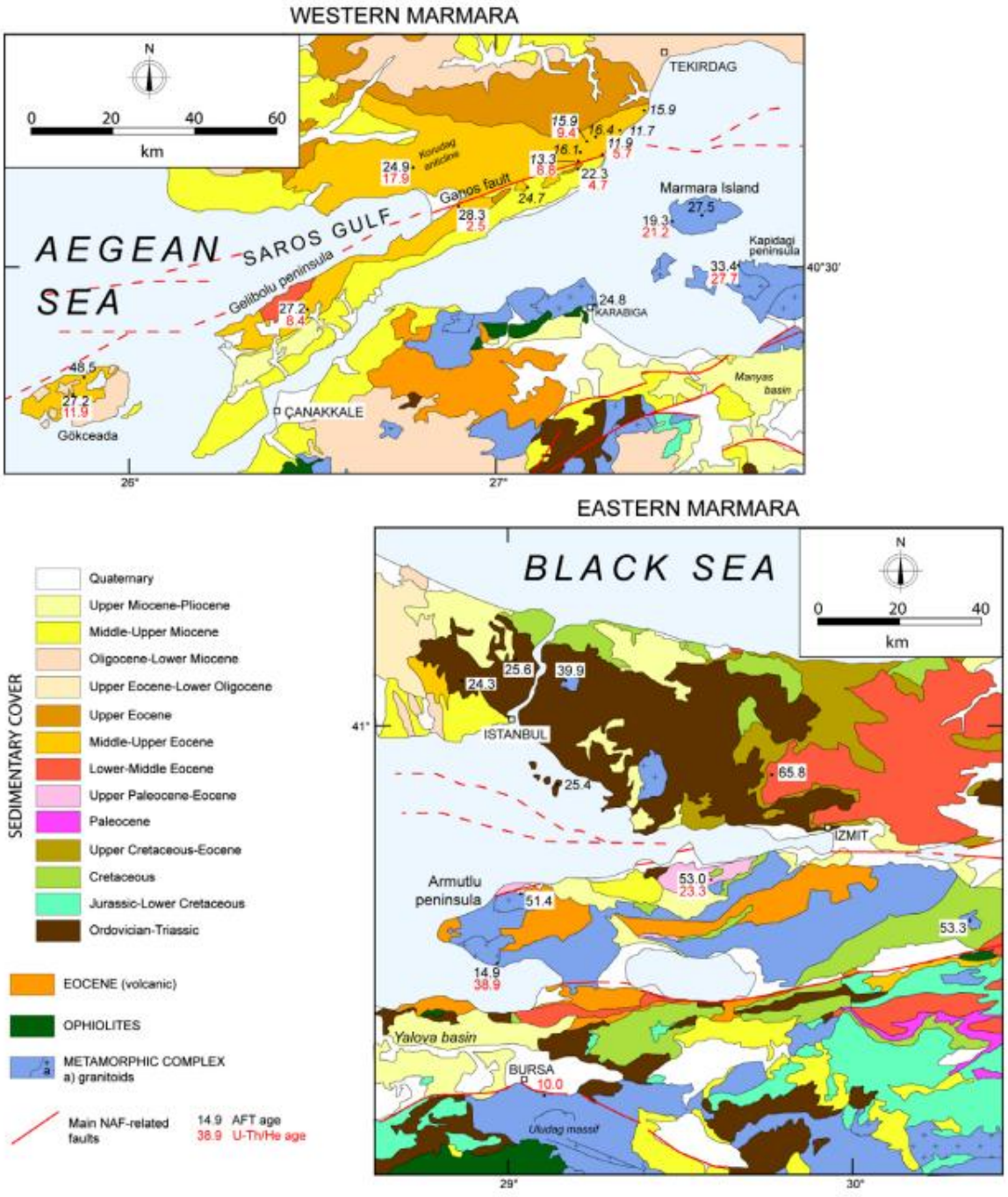

Figure 2.5. Geologic map of Western and Eastern Marmara Region (Zattin *et al.*, 2005).

2.3. Previous Studies

Several seismological, geological, and tectonic studies have been done in the Marmara Region because of its attractive and complex structure, especially after 17 August 1999 İzmit and 12 November 1999 Düzce earthquakes. Among them, the receiver functionstudies mostly focused on the eastern part of the Marmara Region and especially the land area of this region. Hence, the crustal structure from these studies generally represents structure beneath the land area. After installation of the sea bottom observatory stations in the Marmara Sea, it became possible to study crustal structure beneath OBS stations under the Marmara Sea with receiver function.

There are several on-shore studies targeted to obtain crustal velocity variation and structure of the Marmara Region; Gürbüz *et al.,* (1992), Gürbüz *et al.,* (2000), Karabulut *et al.,* (2003), Barış *et al.,* (2005), Zor (2006), Işık (2013).

Gürbüz *et al.,* (1992) determined velocity-depth models beneath 13 stations surrounding the Marmara region by using earthquake travel time data. The study showed that thickness of the crust varies from 27 to 34 km and minimum thickness is seen around Istanbul. According to the study, the thickness increases to the south of Marmara Sea and also it becomes thicker in Trace Region. The results of their study also suggested that there is a gradual increase in crustal thickness from İstanbul to Edincik and crustal structure beneath the Marmara region is too complex. There are also various high velocity seismic zones and some gaps exist in the area. Finally, the study showed that average P wave velocity in the crust and beneath the Moho is 6.2 km/s and 7.9 km/s, respectively. In addition to the study, Gürbüz *et al.,* (2000) computed 1D velocity structure model using 180 events recorded by well distributed land station geometry around the Marmara Sea by using VELEST code. The velocity model is given in Table 2.1.

Table 2.1. Minimum 1D model for the Marmara Region (Gürbüz *et al.,* 2000).

P Wave Velocity (km /s)	Depth (km)
3.0	0.0
5.3	4.8
5.9	9.5
6.2	12.5
6.5	17.0
7.3	24.0
7.9	29.0

Several scientists also revealed the thickness variation of the crust in the Marmara region. Horasan *et al.,* (2002) found the total thickness of the crust is 32 km, and the Pg and Pn velocites are 5.9 and 8.0 km/sec, respectively, in the Gulf of İzmit, Marmara Region.

Karabulut *et al.,* (2003) presented 2D tomographic velocity model in eastern Marmara and they found that the average crustal velocity is around 5.7-5.9 km/s. They also found a relationship with the locations of low velocity zones and strike slip motion of the northern branch of the NAFZ. They related the results with the complex structure of the region. Another crustal structure study for the Marmara Region is a tomographic inversion method by Barış *et al.,* (2005). They showed that western part of NAFZ shows lateral heterogeneity and low velocity values correspond to the sedimentary units or the alluvium regions.

Zor (2006) revealed that the velocity models for the stations installed on the same tectonic units for eastern part of the Marmara Region are significantly similar to each other by applying the receiver function method to the data obtained from the eleven broad-band stations. He also observed that the crustal thickening from west (29-32 km) to east (34-35

km) along the NAFZ. The results of this study showed that the average crustal thickness and S wave velocity for the whole region are 31 ± 2 km and 3.64 ± 0.15 km/s, respectively.

Denli (2008) investigated 3D velocity structure of the Eastern Marmara Region from local earthquake tomography. In his study, generally low velocities vary between 5.3-5.7 km/s through vertical extension ofthe faults and these extensions of the NAF branches are observed between 2-15 km depths. Mutlu (2011) applied Pn tomograhpy in Turkey included Marmara Region and found the thickness of the crust is nearly 30-32 km in that region.

Vanacore *et al.*, (2013) presented the first plate scale Moho and Vp/Vs ratio map of the Anatolian Plate based on H-κ stacking of receiver functions for approximately 300 stations. According to their study, Moho depth increases from west to east and Western Anatolia is dominated by on average shallower Moho depth. They also presented the Moho depth about 28-32 km for the Marmara Region.

The offshore crustal structure studies in the Marmara Sea are done by Bécel (2006); Bécel (2009); Bayrakçı (2009) and Bécel (2006) and Bécel *et al.*, (2009). These studies have revealed that the Moho depth varies horizontally by using WARR and MSCstudies. Bécel *et al.*, (2009) interpreted the EW seismic reflection profile and founda decrease of Moho depth beneath the eastern and western edges of the Marmara Trough. An EW spatial variation in the absolute depth of the Moho of about 5 km is observed as well as a significant increase in basement depth reaching up to 26 km. They also suggested a negative flower structure related to the consistent model of thinning, extension and transition at the scale of the lithosphere. Bayrakçı (2009) estimated the 3D basin structure under the sea by explosion data tomography. Her results give a detailed basin and velocity structure in the Marmara Sea.

The most recent offshore crustal study is Işık (2013). The study suggests that the sediments deposits in the sea show very low velocities as 3-3.5 km/s with almost at the same depths between 5 and 6 km. Furthermore, the lower crust velocity information showed similarities under Central Basin and the Çınarcık Basin. These are surrounded by high velocity zones which can be accepted as an indicator of the normal faulting.

3. RECEIVER FUNCTION METHOD

3.1. Introduction

Receiver functions are used to determine crust and upper mantle structure. Receiver functions are time series that are computed from three-component seismograms and show relative response of Earth structure under a seismic station. The waveform is a composite of P-to-S converted waves that reverberate below the surface (Ammon, 1991). In receiver function technique, teleseismic waveforms which include a series of reflection, refraction, and conversions are often used.

The basic idea of this method is that incoming P wave is converted into SV wave at Moho discontinuity due to the sharp velocity contrast and these converted waves come to the station after direct P wave. Receiver function trace includes the direct P wave, Ps converted and PpPhs phases which have a positive polarity, and PpShs+PsPhs reverberated phase which has a negative polarity.

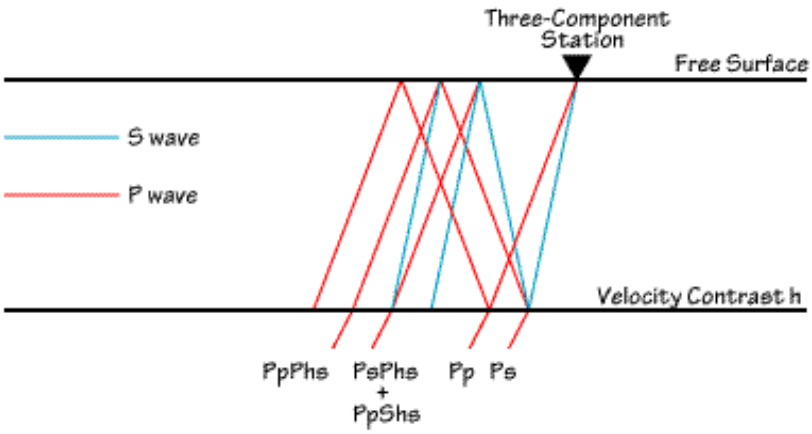

Figure 3.1. Phase arrivals of teleseismic incident P wave for a layer over a half space model (Ammon, 1991).

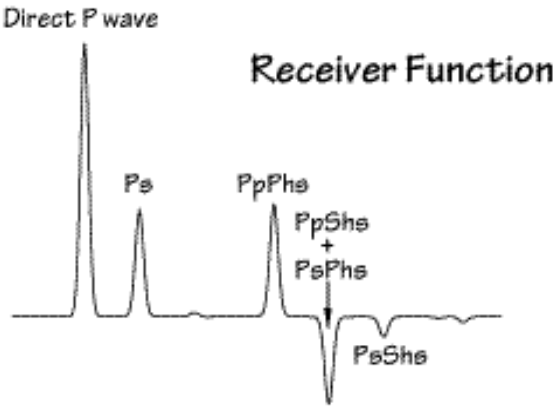

Figure 3.2. Receiver function traces that show direct P, Ps conversions and its multiples, respectively (Ammon, 1991).

The relative amplitudes of the phase arrivals in a receiver function depend on the incidence angle of the impinging P-wave and the size of the velocity contrasts generating the conversions and multiples. Moreover, the arrival times of the converted phase and multiples depend on the depth of the velocity contrast, the P and S velocity between the contrast and the surface, and the P-wave incidence angle, or ray parameter. In addition to all, the amplitudes of the later arrivals and their frequency content depend on the nature of the velocity transition (Ammon *et al.*, 1990).

Both radial and transverse receiver functions can be computed. While radial receiver function is defined as spectral division of the radial and vertical seismograms, transverse receiver function is defined as the spectral division of tangential and vertical seismograms in the frequency domain.

3.2. Receiver Function Analysis

In receiver function studies, teleseismic events which are ranging from 30° to 90° are commonly used because P waves are steeply incident and dominate vertical component of ground motion whereas Ps converted phases are recorded on the horizontal component dominantly in this range (Cassidy, 1992). Generally, three component broad-band seismometers are preferred to use because they have a flat velocity response throughout

most of the lower frequency bands in contrast to the spectrum of short period seismometers.

After selecting the teleseismic events, the next step is filtering of the waveforms to obtain high quality data and eliminate high frequency content which are affected by small-scale heterogeneities. 0.1 Hz-1 Hz or 0.05 Hz-1 Hz are suitable for filtering of teleseismic events. Another step is windowing of seismograms and it depends on the discontinuities of interest. In this study, 10 seconds before P wave arrival and 50 seconds after P wave arrival is applied.

The following step in receiver function analysis is to rotate the filtered and windowed teleseismic events. By using the back azimuth, the angle measured between the vector pointing seismic station to source and seismic station to north (Scherbaum and Johnson, 1992), the North-South (NS) and East-West (EW) components can be rotated into the radial and tangential components, respectively (Figure 3.3). The reason why we use the ray based (RT) system is that P to SV converted phases are radially polarized and observed on radial component, while P to SH converted phases are transversally polarized and observed on tangential component.

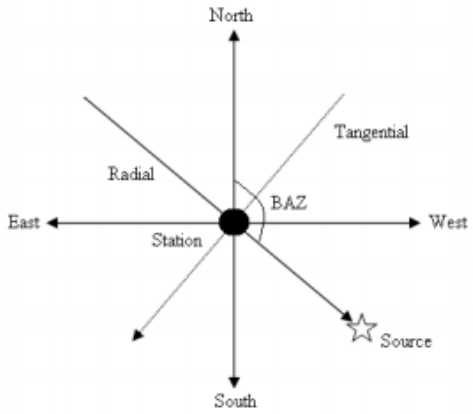

Figure 3.3.The back-azimuth (BAZ) (Zor, 2002).

Filtering, windowing, and rotating can be seen in the following Figure 3.4. The first figure represents raw waveform downloaded from IGDM station. The other one shows the results of filtering, windowing and rotating steps for the same event.

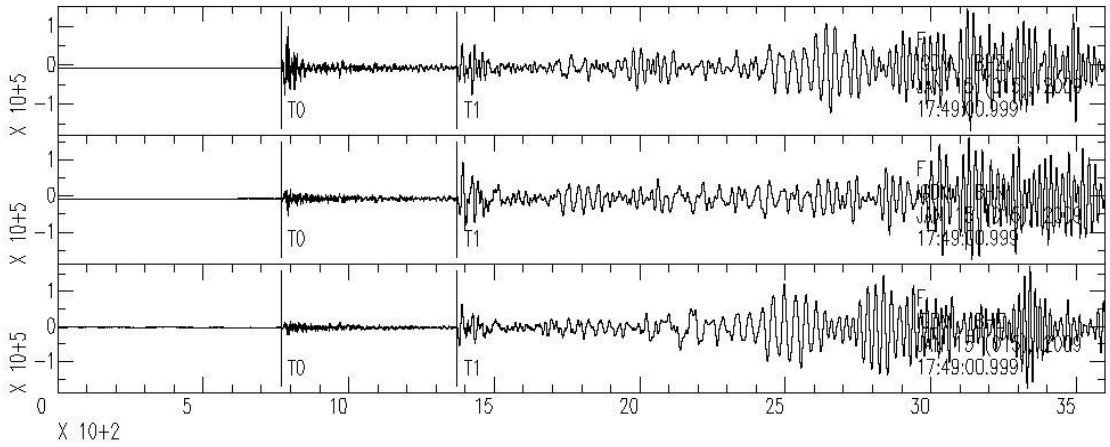

(a)

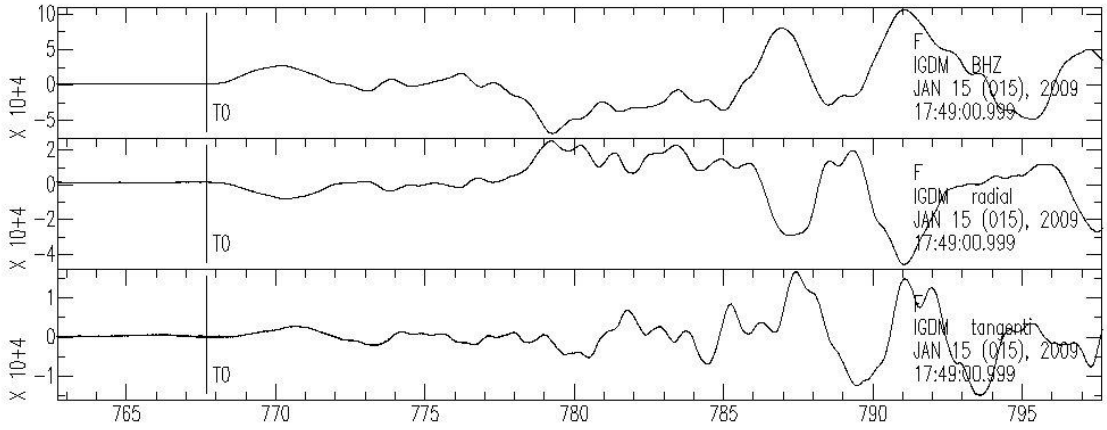

(b)

Figure 3.4. The original three component waveform recorded at IGDM station (15 January 2009, Mw. = 7.4) a) Raw data. b) After filtering, windowing and rotating of the first 30 seconds of the seismic trace after P wave onset time.

The final step in receiver function analysis is to obtain radial and tangential receiver functions from filtered, windowed, and rotated teleseismic waveforms. By applying deconvolution which means spectral division of the radial and transverse components to vertical component, the estimation of receiver functions can be done. In addition, the aim of this procedure is to eliminate the effects of the near source ray path and instrument response in order that we can obtain the signal which includes the first P wave, P-to-S wave conversions, and locally generated reverberations under the station.

Deconvolution process can be completed either in frequency domain which was proposed by Langston (1979) or in time domain proposed by Ligorria and Ammon (1999).

3.2.1. Frequency Domain Deconvolution

Frequency domain deconvolution process was developed by Phinney (1964) and Langston (1979) extended this technique by using a water-level stabilization method and a low-pass Gaussian filter.

The theoretically calculated displacement response *D(t)* is computed by convolving of instrumental response I(t), the seismic source time function *S(t)*, and the impulses responses $E_V(t)$, $E_R(t)$, and $E_T(t)$ which are the vertical, radial, and tangential components. This deconvolution process for a P plane wave impinging under stack of horizontal or dipping interfaces is given by

$$D_V(t) = I(t) * S(t) * E_V(t) \tag{3.1}$$

$$D_R(t) = I(t) * S(t) * E_R(t) \tag{3.2}$$

$$D_T(t) = I(t) * S(t) * E_T(t) \tag{3.3}$$

At teleseismic distances, 30°-90^0, we assume that $E_V(t)$ is a Dirac delta function because the vertical component is composed of a steeply incident P wave consist of large direct arrivals followed by small arrivals from crustal reverberations in this range.

$$E_v(t) \approx \delta(t) \tag{3.4}$$

Thus, the vertical component response can be represented by

$$D_V(t) \approx I(t) * S(t) \tag{3.5}$$

Therefore, radial receiver function which is radial component of earth response can be calculated by deconvolving vertical component $D_V(t)$ with radial component $D_R(t)$.

Similarly, tangential receiver function can be computed by deconvolving from tangential component $D_T(t)$. Radial and transverse receiver functions in frequency domain are obtained by

$$E_R(\omega) = \frac{D_R(\omega)}{I(\omega)S(\omega)} \approx \frac{D_R(\omega)}{D_V(\omega)} \tag{3.6}$$

$$E_T(\omega) = \frac{D_T(\omega)}{I(\omega)S(\omega)} \approx \frac{D_T(\omega)}{D_V(\omega)} \tag{3.7}$$

$E_R(\omega)$ and $E_T(\omega)$ are radial and tangential receiver functions and they can be retransformed back into the time domain. For the purpose of making dominator real in Equation 3.6, we can multiply denominator with complex conjugate $D_V^*(\omega)$ and radial receiver function is equal to,

$$E_R(\omega) = \frac{D_R(\omega)D_V^*(\omega)}{D_V(\omega)D_V^*(\omega)} \tag{3.8}$$

A similar equation can be defined for the tangential receiver function $E_T(\omega)$. The Equation 3.8 is multiplied by the low Gaussian filter $G(\omega)$ so as to remove high frequency noise from receiver functions and smooth the results.

$$E_R(\omega) = \frac{D_R(\omega)D_V^*(\omega)}{D_V(\omega)D_V^*(\omega)} G(\omega) \tag{3.9}$$

$$G(\omega) = e^{-\omega^2/4\alpha^2} \tag{3.10}$$

In Equation 3.10, α controls the width of the Gaussian filter and it is used to remove high-frequency noise.

Table 3.1. The values of α and corresponding frequency values at which $G(\omega)$ is equal to 1.

α values	Frequency(Hz)
10	4.8
5	2.4
2.5	1.2
1.25	0.6
1.0	0.5
0.625	0.3
0.5	0.24
0.4	0.2
0.2	0.1

The division of deconvolution in frequency domain can cause some numerical problems in calculations for the case of small or zero values of $D_V(\omega)\ D_V^*(\omega)$. Therefore receiver function which is defined as in Equation 3.8 is not used to compute the radial response of the earth. Thus, a water-level deconvolution technique developed by Helmberger and Wiggins (1971) and (Dey-Sarkar and Wiggins, 1976) can be used to avoid this problem.

$$E_R(\omega) = \frac{D_R(\omega) D_V^*(\omega)}{\Phi_{SS}(\omega)} G(\omega) \tag{3.11}$$

$\Phi_{SS}(\omega)$ represents autocorrelation of $D_V(\omega)$ with any spectral troughs filled to a level depending on the water level parameter, c and it is used to replace small values in Equation 3.12 with a fraction of the maximum value of the denominator. The consequence of replacing small values with larger ones in the denominator is an attenuation of spectral energy at frequencies for which the vertical component has small amplitude (Ammon, 1991).

$$\Phi_{SS}(\omega) = \max\{D_V(\omega)D_V^*(\omega), c\max[D_V(\omega)D_V^*(\omega)]\} \quad (3.12)$$

Water level parameter is ranging from 0.0001 to 0.1 and it should be chosen by comparing the results of several trial water-level fractions until reaching to an ideal result. Since the water level filter can cause distortions in calculations, choosing smaller values can give better results.

The averaging function, which is computed by deconvolving the vertical component of motion from itself, can be calculated to show the effects of the water-level parameter and Gaussian filter on the waveform. However, large water-level values produce a broadened and often distorted averaging function (Ammon, 1991).

3.2.2. Iterative Time Domain Deconvolution

In receiver function studies, the type of seismic data used to analyse is very important. Unless the signal to noise ratio is small, iterative time domain approach can be used to obtain more reliable receiver functions with respect to frequency domain technique.

This deconvolution method is a least square minimization of the difference between observed horizontal seismogram and a predicted signal generated by the convolution of an iteratively updated spike train with the vertical component seismogram (Ligorria and Ammon, 1999).

In order to determine the lag of the first and largest spike in the receiver function, the vertical component is cross-correlated with radial component. The spike amplitude is calculated by solving a simple equation included in Kikuchi and Kanamori (1982). Then the convolution of the current estimate of the receiver function with the vertical-component seismogram is subtracted from the radial-component seismogram. This process estimates the misfit, and when the procedure is repeated for more spikes and amplitudes, each additional spike reduces the misfit. The iteration will go on until the reduction in misfit with additional spikes becomes unimportant (Ligorria and Ammon, 1999).

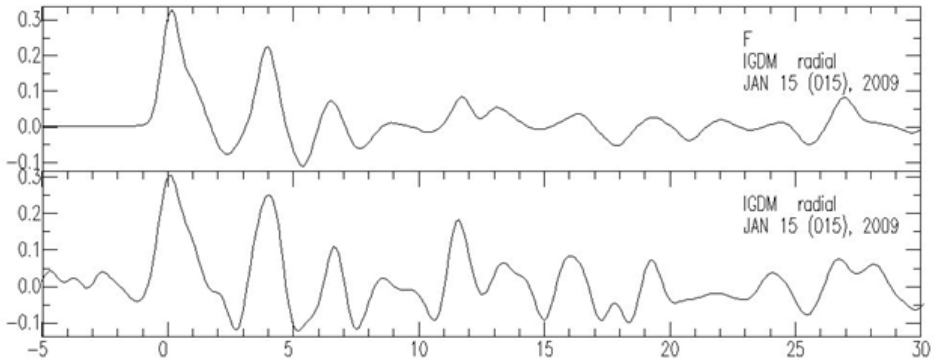

Figure 3.5. A comparison of two radial receiver functions which are obtained from iterative time domain deconvolution (top) and frequency domain deconvolution (down).

3.3. Receiver Function Techniques

3.3.1. H-κ Stacking Technique

In receiver function, the converted phasePs and reveberated phases of PpPs and PpPs + PsPs carry relevant information in respect to the crustal properties such as H and Vp/Vs ratio. They are important parameters to understand the crustal structure, which can be determined beneath a station if the above mentioned phases are clearly observed.

A useful technique to calculate depth and Vp/Vs ratiowhich became popular in the last decade is called H-k stacking method and it was proposed by Zhu and Kanamori (2000). It is assumed inthis method that the crust is laterally uniform and consisting of laterally horizontal layers.

The time difference between Ps and P can be used in receiver function analysis to calculate average crustal thickness

$$H = \frac{t_{Ps}}{\sqrt{\frac{1}{V_s^2} - p^2} - \sqrt{\frac{1}{V_p^2} - p^2}} \tag{3.13}$$

where H is the thickness, p is ray parameter, Vp and Vs are average crustal velocities, and t_{ps} is the time seperation between P and Ps arrival times.

Additionally, the crustal thickness can be estimated by using the arrival time of the reverberated phase PpPs,

$$H = \frac{t_{PpPs}}{\sqrt{\frac{1}{V_s^2} - p^2} + \sqrt{\frac{1}{V_p^2} - p^2}} \tag{3.14}$$

And also for other reverberated phases PpSs + PsPs

$$H = \frac{t_{PpSs+PsPs}}{2\sqrt{\frac{1}{V_s^2} - p^2}} \tag{3.15}$$

In real situations, it is not easy to observe converted Ps phase and the multiples PpPs and PpSs + PsPs on a receiver function trace because of background noise, scattering from crustal heterogeneties, and P to S conversions from other velocity discontinuties. Therefore, stacking multiple events in the time domain can be helpful in order to increase the signal to noise ratio.

However, Zhu and Kanamori (2000) have developed a H-κ stacking tecnhique that sums the amplitudes of receiver function at the predicted arrival times of Ps, PpPs and PpSs + PsPs for different crustal thickness H and κ values. Figure 3.6 indicates that curves showing the contributions of Ps and its two major crustal multiples (PpPs and PpSs + PsPs) to the stacked amplitude as a function of crustal thickness and Vp/Vs ratio.This tecnique makes a transformation from the time domain receiver functions directly into the H-Vp/Vs domain without the need of identfiying reverberated phases at Moho and picking their arrival times with assuming a starting average P wave velocity. H-κ stacking is described as:

$$s(H\text{-}\kappa) = \sum_i w_1 rf_i(t_1) + w_2 rf_i(t_2) - w_3 rf_i(t_3) \tag{3.16}$$

where $rf_j(t)$ is the radial receiver function with j ranging from one to the total numbers of waveforms. H is the thickness; κ is the Vp/Vs ratio. t_1, t_2, and t_3 are the predicted Ps, PpPs and PpPs + PsPs arrival times corresponding to crustal thickness. H and Vp/Vs ratio (κ) are given in the equations between 3.13 and 3.15. The w_1, w_2, and w_3 are the weighting factors and $w_1 + w_2 + w_3 = 1$.

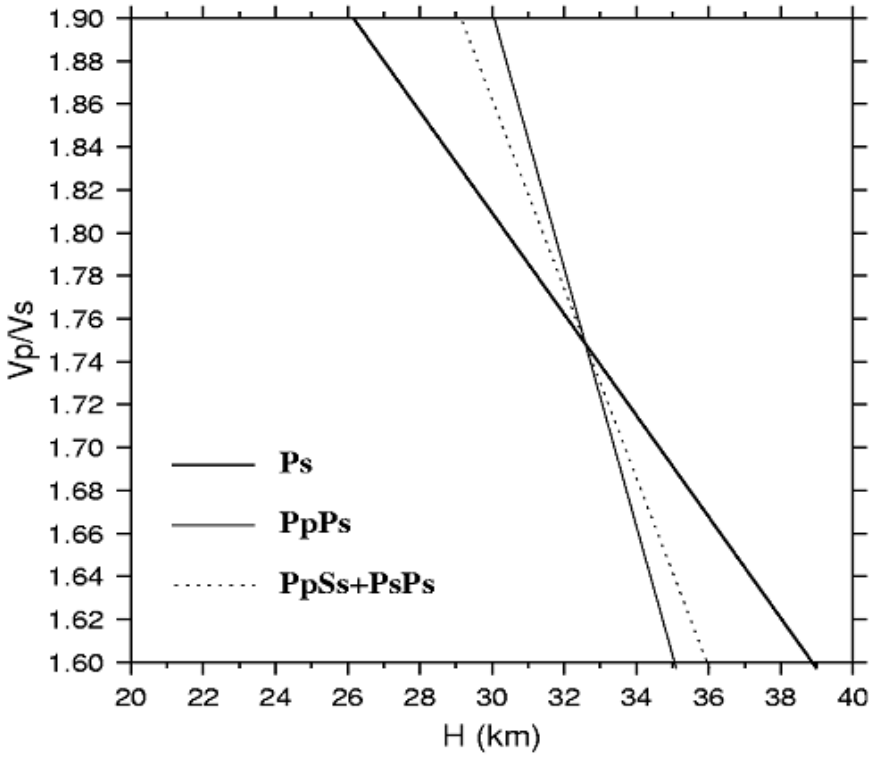

Figure 3.6. Curves showing the contributions of Ps and its two major crustal multiples (PpPs andPpSs+PsPs) to the stacked amplitude as afunction of crustal thickness and Vp/Vs ratio.

According to the Zhu and Kanamori (2000), the weight for Ps should be greater than the sum of the weights of PpPs and PpPs + PsPs to balance the contribution for three phases. The default values in their study weretaken as 70%, 20% and 10%. They also stated that Ps has the highest signal-to-noise ratio, therefore it should be given a high weight factor than Ps, PpPs and PpPs + PsPs. The best estimation of H and κ are found when these phases are stacked coherently.

An advantage of this algorithm is that large amounts of teleseismic waveforms can be conveniently processed. In addition, estimation of crustal thickness or Vp/Vs ratio do not contain effect of lateral variations since Ps conversion point is very close to the station. Moreover, average crustal model is obtained by stacking receiver functions from different distances and directions, and there is no need to pick arrival times of different conversion phases (Zhu and Kanamori, 2000).

On the other hand, the method has some limitations. One of them is that Moho discontinuity is assumed planar, homogeneous, and there is no lateral variation. However, if Moho is dipping then it affects Vp/Vs ratio that indicates lateral heterogeneities. Dipping of this interface will cause travelling of waves larger distances through the crust and will have longer travel times, with respect to those generated at a horizontal interface (Ligorria, 2000). Rays travelling along or downdip direction, the differential arrival times of Ps and multiples generated at dipping Moho are smaller than those generated at flat Moho and make the H-κ stacking results deviate from the model structure.

Another disadvantage is that the presence of a gradational crust-mantle boundary instead of a sharp, well defined Moho discontinuity (Julia, 2004). This type of boundary makes the energy from the boundary interaction phases that spread in time so that the corresponding pulses decrease in amplitude and increase in width (Cassidy, 1992; Liggoria, 2000). In addition to this, converted phases and multiples from intra-crustal discontinuities could interfere with the real Moho Ps converted phase. Especially in sedimentary environments where the multiples from the sediment–bedrock interface overlap in time with the Ps converted phase at the Moho (Cassidy, 1992; Zelt & Ellis, 1998). As a result, time shift of the Ps peak may lead to unrealistic thickness and V_P/V_S ratios.

3.3.2. Linearized Iterative Inversion Method

Linearized Iterative Inversion Method introduced by several scientists. Among these types of inversions the most popular one is introduced by Ammon *et al.*, (1990). Building upon the inversion method of Owens *et al.*, (1984) Ammon *et al.*, (1990) implemented the efficient algorithm of Randall (1989) for calculating differential

seismograms and the jumping inversion technique of Shawand Orcut (1985). Ammon et *al*., (1990) pointed out that inversion results are strongly dependent on the selection of initial models. A suitable initial model can lead the inversion procedure to a result very close to the true solutionwith only several iterations. Therefore, how to acquire suitable initial models is the key for solving linearized inverse problems.

Receiver function inversion is used to obtain crustal velocity structures from information contained in the waveforms. The forward problem can be expressed in the equational form, m represent the velocity model, dm a velocity correction vector, d the residual vector, and G the matrix whose i'th column is the partial derivative of the receiver function with respect to the shear velocity in layer (i). The initial model is called m_o and the model which is sought is called m, where $m = m_o + dm$.

$$G\,dm = d \tag{3.18}$$

By adding Gm_o to both sides

$$G\,dm + G\,m_o = d + Gm_o \tag{3.19}$$

and by using the fact that $m = m_o + dm$, it can be constructed another Equation (3.20) and inverted directly for the model, m.

$$Gm = d + Gm_o \tag{3.20}$$

Inverting the Equation (3.19) above for the correction vector, dm, is called creeping, inverting the Equation (3.20) directly for m is called jumping. A singular-value decomposition is computed the matrix inverse and solve the inverse problem in this method.

4. DATA ANALYSIS

4.1. Data and Seismic Stations

In Marmara Region, a total of 45 permanent broad-band seismic stations were used to investigate the crustal structure of the area. 21 seismic stations and five SBO stations are belong to KOERI, 17 stations were deployed by TUBITAK and two are the project based stations. Figure 4.1 shows stations used in this study.

In our study, data format differs from stations to stations depending on the type of recording equipments used in the seismic station. We used SAC program to analyze the waveforms, therefore sac data format is needed. Reftek data were converted first to seg-y format and later to sac data format. Furthermore, data collected from Güralp instruments of which are at gcf format were converted to sac format to analyze the data set. Station list is given in Table 4.1.

In this study, we processed teleseismic data which is collected between January, 2008 and September, 2012. Approximately 250 teleseismic events were chosen from the USGS earthquake catalog according to magnitudes (Mw) greater than 5.5 and epicentral distances ranging from 30^0 to 90^0 degrees. The distrubition of events are given in Figure 4.2. We calculated receiver functions using a time-domain iterative deconvolution for each station using vertical and radial seismograms. We could not use all the earthquakes recordings due to the elimination of events with low signal to noise ratio, operation of stations at different times or technical problems at some seismic stations. For this reason, we used 35 stations and selected signals better than 80% misfit between predicted and actual radial receiver function which is a valuable parameter to identify problematic deconvolutions.

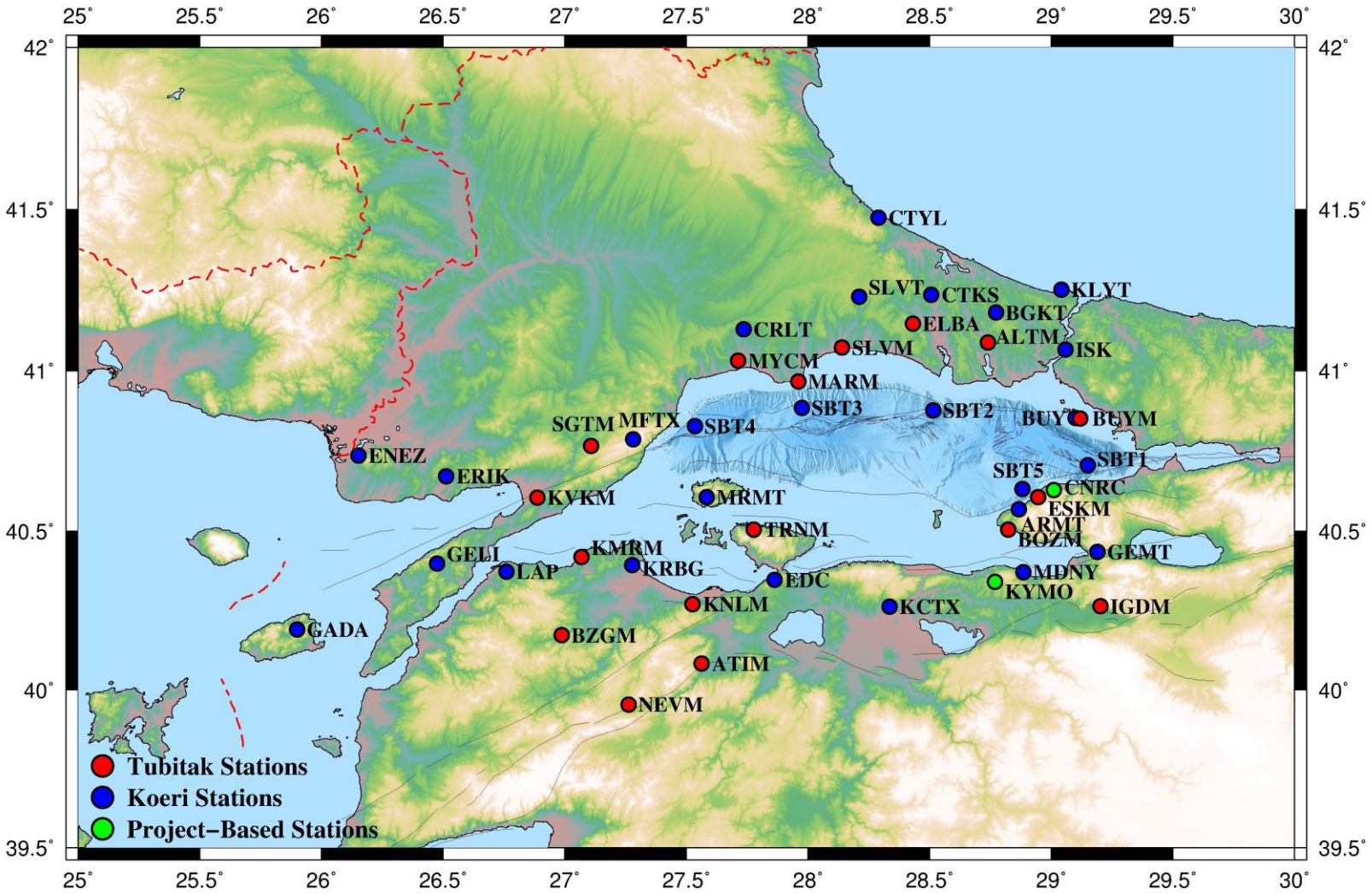

Figure 4.1. Stations used in this study.

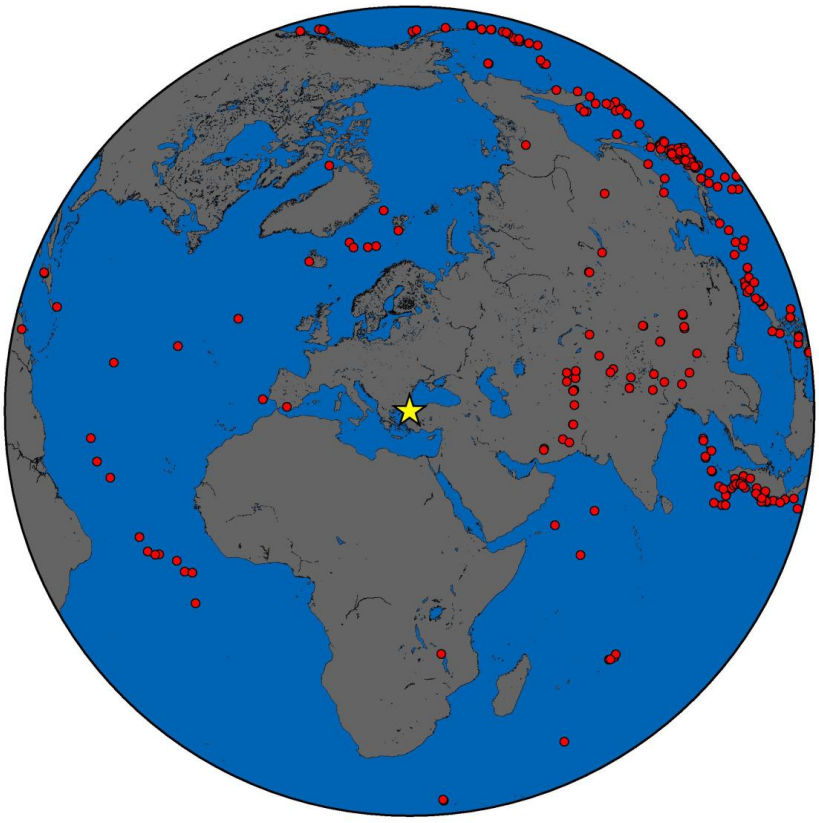

Figure 4.2. Location of teleseismic earthquakes used in this study.

After selecting the available data, basic preparation steps were applied to the data. Firstly, P arrival times of earthquakes were picked by hand and the data were cut with windowing from 60 seconds before P arrivals to 90 seconds after the predicted P arrival time. Then a band-pass filter 0.01-2 Hz is applied to the observed seismograms to enhance S/N ratio. To isolate converted S phases from the P wave, XYZ components are transformed into RTZ coordinate system by using backazimuth. After these steps, the iterative time domain deconvolution (Ligorria and Ammon, 1999) is performed to obtain receiver functions by using 200 iterations and a gaussian width factor of 2.0. The azimuthal coverage is mostly between the back-azimuth of 0^o and 110^o for our region. The whole procedure is shown in Figure 4.3 as a flow chart.

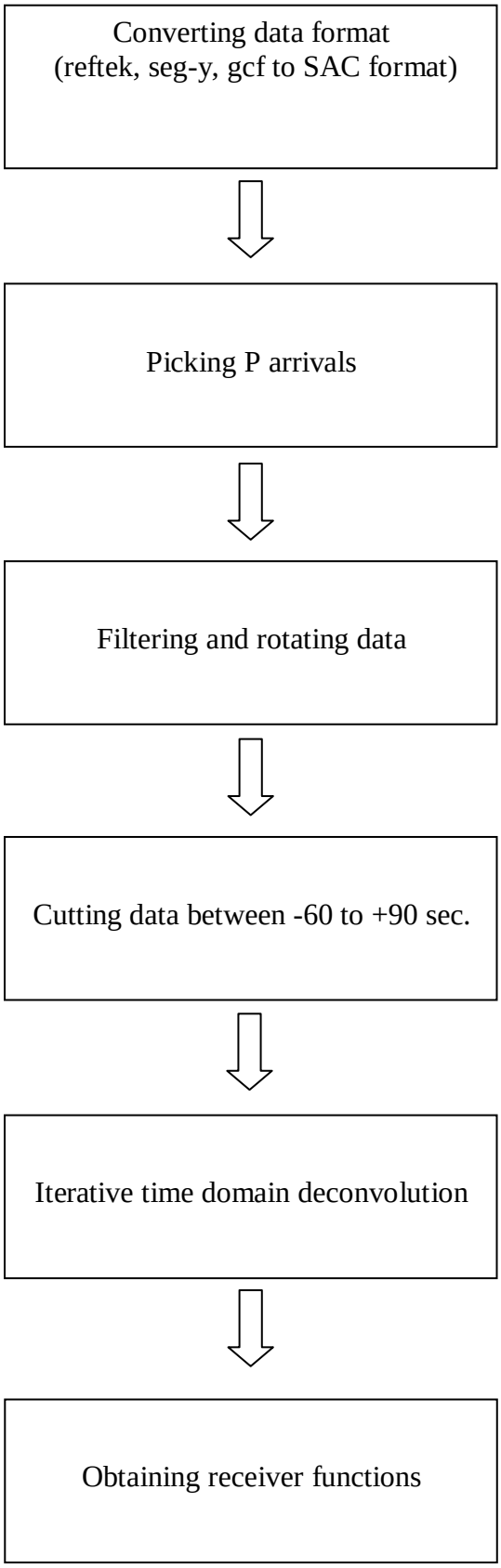

Figure 4.3. Basic steps in data analysis.

Table 4.1. Information about seismic stations used in this study.

CODE	SENSOR	LAT	LON
ALTM	3ESPC	41,0880	28,7400
ARMT	3ESP	40,5683	28,8660
ATIM	3T	40,0830	27,5633
BGKT	3ESP	41.1810	28.7730
BOZM	3ESPC	40,5340	28,7820
BUY	3ESP	40,5340	28,7820
BUYM	3T	40,8523	29,1180
BZGM	40T	40,1727	26,9865
CNRC	3T	40,6277	29,0111
CRLT	3ESP	41,1290	27,7360
CTKS	3ESP	41,2373	28,5072
CTYL	3T	41,4760	28,2897
EDC	3T	40,3465	27,8618
ELBA	3T	41,1467	28,4305
ENEZ	3T	40,7362	26,1530
ESKM	3T	40,6068	28,9453
ERIK	3ESP	40,6708	26,5132
GADA	3T	40,1908	25,8987
GELI	3ESP	40,3980	26,4742
GEMT	3T	40,4350	29,1890
IGDM	3ESPC	40,2640	29,2013
ISK	3T	41,0657	29,0592
KCTX	3ESP	40,2627	28,3353
KLYT	3T	41,2530	29,0420
KMRM	3ESPC	40,4180	27,0690
KNLM	3T	40,2700	27,5260
KRBG	3ESP	40,3932	27,2977
KVKM	3T	40,6040	26,8876
KYMO	3T	40,3408	28,7688

LAP	3ESP	40,3703	26,7593
MARM	3T	40,9670	27,9610
MDNY	3ESP	40,3710	28,8847
MFTX	3ESP	40,7867	27,2812
MRMT	3T	40,6090	27,5832
MYCM	40T	41,0325	27,7133
NEVM	3ESPC	39,9540	27,2630
SBT1	3T	40,7042	29,1517
SBT2	3T	40,8783	28,5133
SBT3	3T	40,8850	27,9783
SBT4	3T	40,8283	27,5350
SBT5	3T	40,6311	28,8804
SGTM	40T	40,7668	27,1078
SLVM	3T	41,0731	28,1403
SLVT	3ESP	41,2300	28,2100
TRNM	40T	40,5050	27,7780

4.2. Results of H-κ Analysis

After obtaining receiver function with deconvolution process, some receiver functions which have not clearly observed converted and multiple phases because of low signal to noise ratio were eliminated. Radial and transverse receiver functions used in this study which the Ps converted and their multiples are clearly seen are plotted according to their BAZ for each station in a time window between -5 to 30 seconds in MATLAB®. Radial and transverse receiver functions, teleseismic events and their BAZ used in this study for one Ocean Bottom station (SBT1) are given as an example in Figure 4.4. Generally earthquakes come from all directions for the seismic stations in Marmara Region. However, azimuthal coverage is dominantly between the back-azimuth of 0 and 110 degree. When the phases on receiver function traces which are plotted for stations are considered, several phases can be identified. Ps converted phase has the largest amplitude after the direct P wave arrival, and the first positive phases observed at all stations are between 4 and 5 seconds. The multiple phases PpPs and PpSs generated between Moho and surface are clearly seen at 14-18 and 20-22 seconds, respectively. If a station is installed in sediment basement, phases can be seen immediately after direct P wave. In the case of the stations installed in crystalline basement, this phase can not be observed. On the other hand, lower crustal multiples (LCM) in some stations can be observed about 10 seconds on receiver functions. This phase can be seen between the converted Ps and multiples phases of Moho.

In the next step, in order to determine the crustal thickness and Vp/Vs ratios H-κ method has been applied to receiver functions. The H-κ stacking method proposed by Zhu and Kanamori (2000) involves the summation over the receiver functions of the weighted amplitudes of each phase at the predictedarrival times for different values of H and κ as explained in details in Chapter III. In this method, receiver functions from different distances can be stacked with corresponding ray parameters. In addition to the ray parameter, a fixed P wave velocity in the crust is an important parameter to identify the variation of thickness. In this study Vp value was chosen 6.3 km/s according to previous studies.

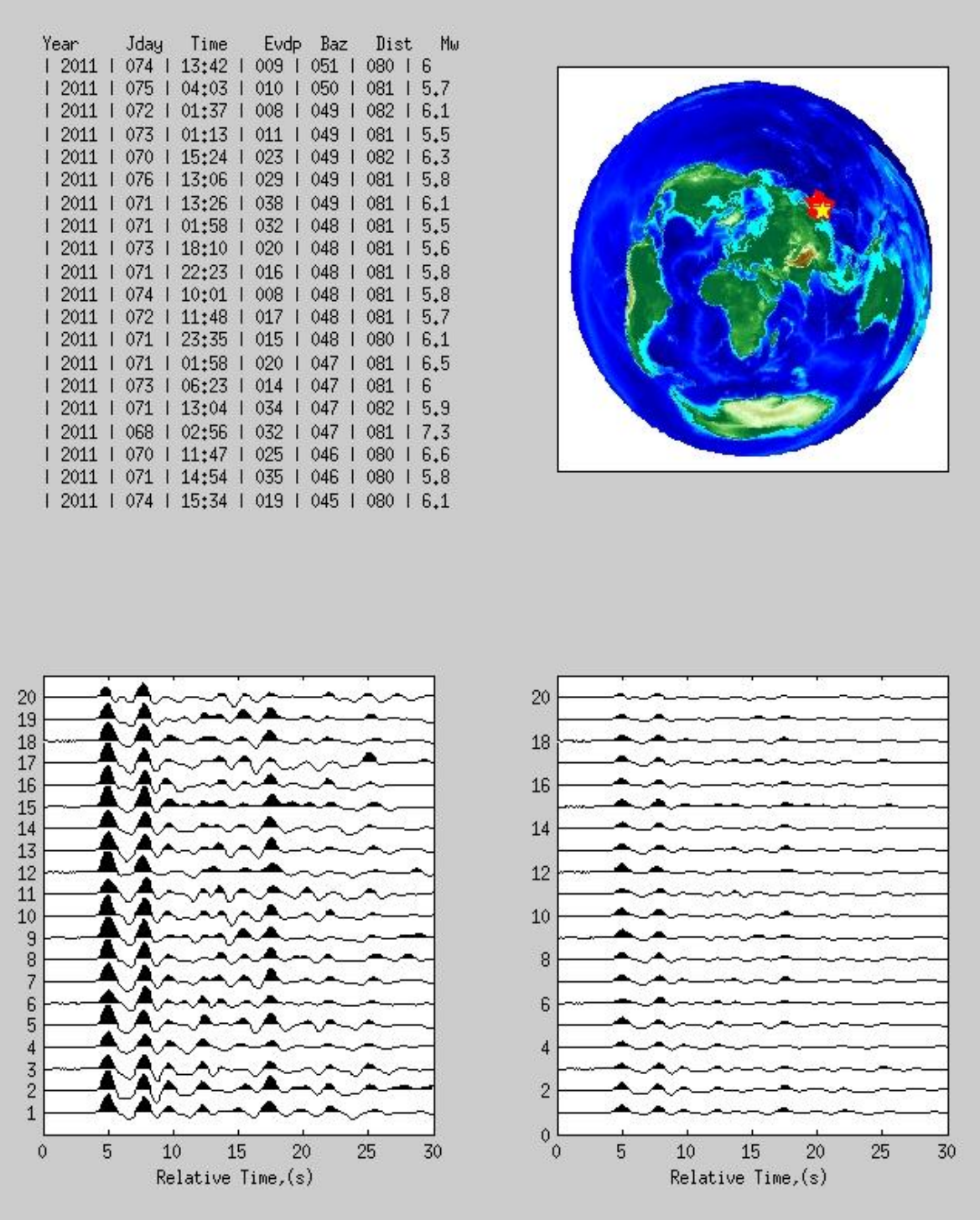

Figure 4.4. Radial and transverse receiver functions of SBT1 station, events used in the analysis and their BAZ map.

The receiver function traces which are obtained can vary with the directions according to the location of seismic stations in different tectonic regions. Therefore, to analyze the receiver functions separately in terms of their dominant BAZ range can be more informative. However, an average crustal estimation for each station can be obtained by applying the method to all RFs from different distances and directions. For this reason, we prefer to use all RFs in this technique. Another step is to select weighting parameters. In this study, these parameters w1, w2, and w3 were chosen 0.7, 0.2, and 0.1 according to visibility of the converted Ps phase and its multiples PpPs, PpSs, respectively. As a consequence, all receiver functions were stacked by using all parameters as mentioned above and the crustal thickness and Vp/Vs ratio can be found stacking three phases coherently.

After the whole procedure cited above, H-κ stack analysis were applied to all stations and crustal thickness and Vp/Vs ratio were found. H-κ stack analysis for each station is represented in Figure 4.5 to Figure 4.12. Stacking results are shown and crustal thickness and Vp/Vs ratios are given in Table 4.2. Finally, Contour map of Moho depth and Vp/Vs ratio map were plotted in Figure 4.13 and Figure 4.14 respectively.

Table 4.2. Depth (H) and Vp/Vs ratios for each station.

CODE	LAT	LON	H	Vp/Vs
ALTM	41,0880	28,7400	33.797±0.62	1.635±0.02
ARMT	40,5683	28,8660	32.939±1.34	1.671±0.04
ATIM	40,0830	27,5633	30.597±0.33	1.819±0.02
BGKT	41.1810	28.7730	32.151±0.33	1.708±0.01
BOZM	40,5340	28,7820	32.506±0.33	1.674±0.02
BUYM	40,8523	29,1180	32.110±0.48	1.640±0.01
BZGM	40,1727	26,9865	31.294±0.6	1.700±0.03
CTKS	41,2373	28,5072	32.744±0.33	1.732±0.02
CTYL	41,4760	28,2897	33.348±0.62	1.780±0.03
EDC	40,3465	27,8618	32.500±0.48	1.717±0.01
ELBA	41,1467	28,4305	32.798±0.62	1.609±0.02
ENEZ	40,7362	26,1530	28.129±0.33	1.962±0.02
ESKM	40,6068	28,9453	32.354±0.39	1.749±0.01
ERIK	40,6708	26,5132	32.795±0.5	1.701±0.02
GADA	40,1908	25,8987	32.465±0.48	1.851±0.02
GELI	40,3980	26,4742	32.645±0.6	1.878±0.03
GEMT	40,4350	29,1890	32.997±0.62	1.775±0.02
IGDM	40,2640	29,2013	32.246±0.77	1.748±0.02
ISK	41,0657	29,0592	29.299±0.62	1.863±0.02
KCTX	40,2627	28,3353	28.388±0.62	1.743±0.02
KLYT	41,2530	29,0420	30.052±0.33	1.965±0.03
KMRM	40,4180	27,0690	33.896±0.62	1.921±0.03
KNLM	40,2700	27,5260	31.949±0.48	1.750±0.03
LAP	40,3703	26,7593	30.303±0.62	1.967±0.03
MARM	40,9670	27,9610	27.308±0.33	1.925±0.01
MDNY	40,3710	28,8847	33.499±0.33	1.695±0.02
MFTX	40,7867	27,2812	33.401±0.06	1.987±0.02
MYCM	41,0325	27,7133	32.404±0.77	1.747±0.02
NEVM	39,9540	27,2630	31.496±0.6	1.730±0.03

SBT1	40,7042	29,1517	32.902±0.62	1.691±0.03
SBT4	40,8283	27,5350	25.999±0.62	1.637±0.03
SBT5	40,6311	28,8804	31.045±0.77	1.690±0.02
SGTM	40,7668	27,1078	33.899±0.66	1.807±0.03
SLVM	41,0731	28,1403	30.846±0.48	1.806±0.02
TRNM	40,5050	27,7780	27.299±0.33	1.696±0.02

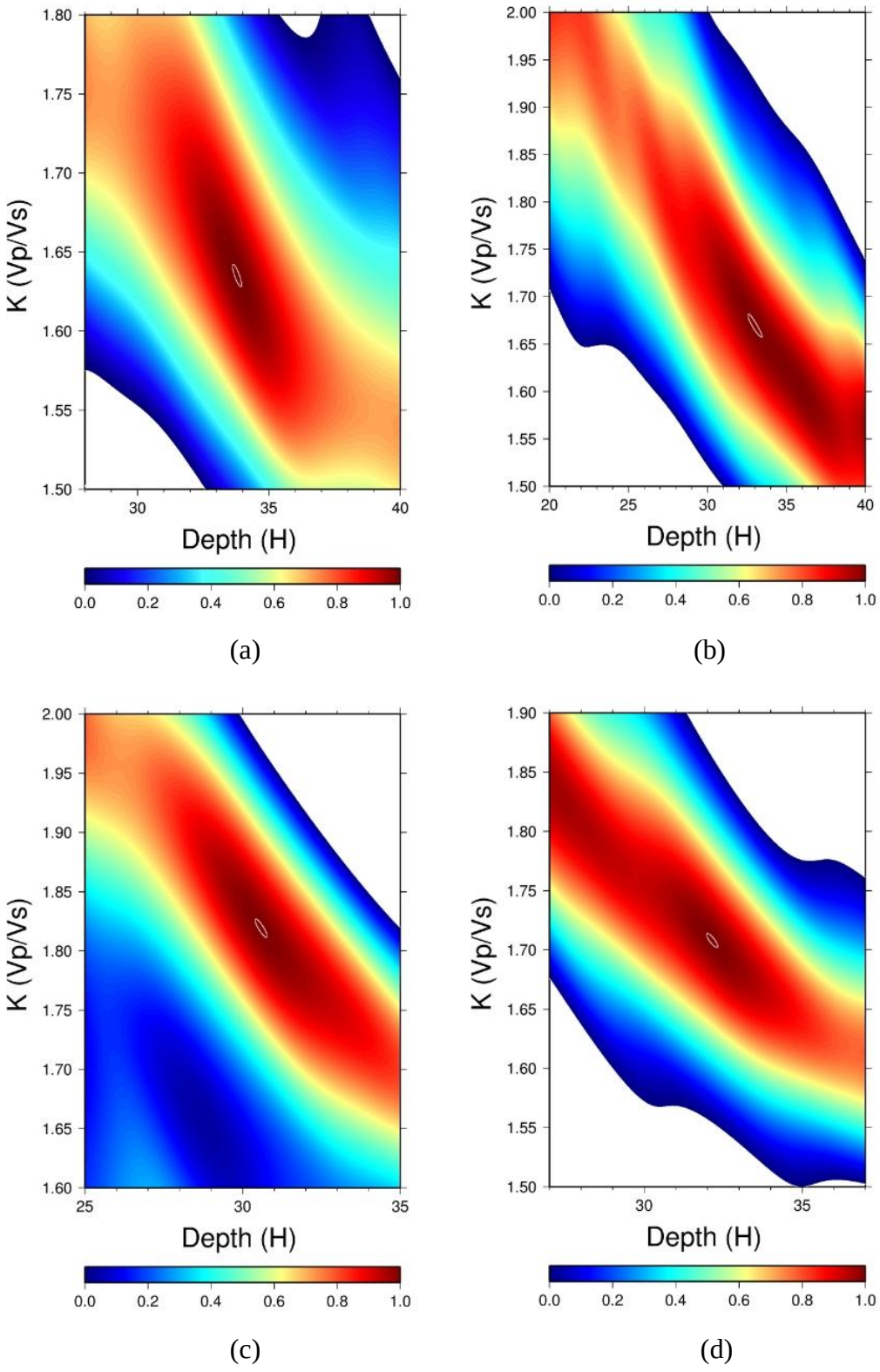

Figure 4.5. H-κ stacking result maps for stations a) ALTM, b) ARMT, c) ATIM and d) BGKT.

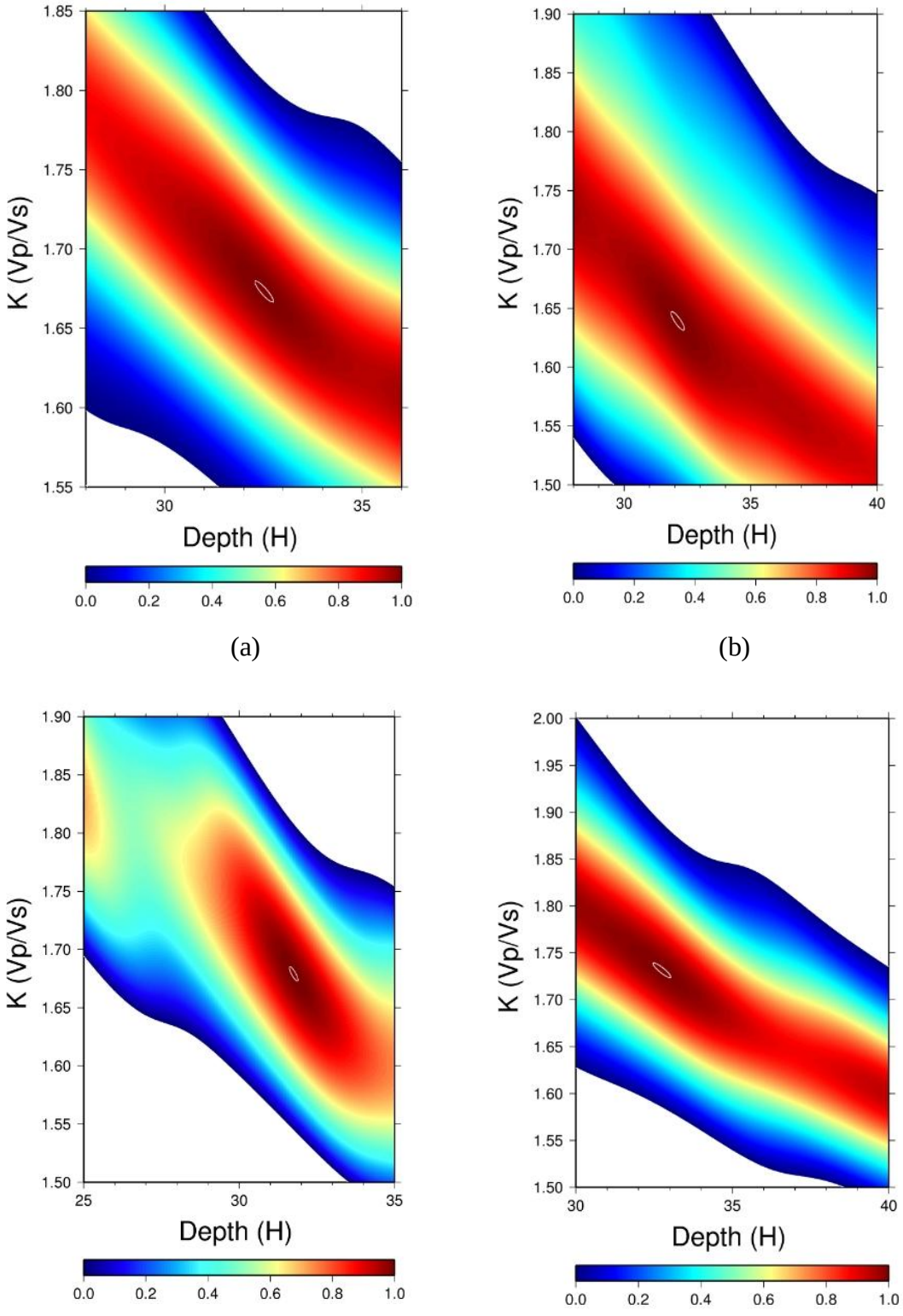

Figure 4.6. H-κ stacking result maps for stations a) BOZM, b) BUYM, c) BZGM and d) CTKS.

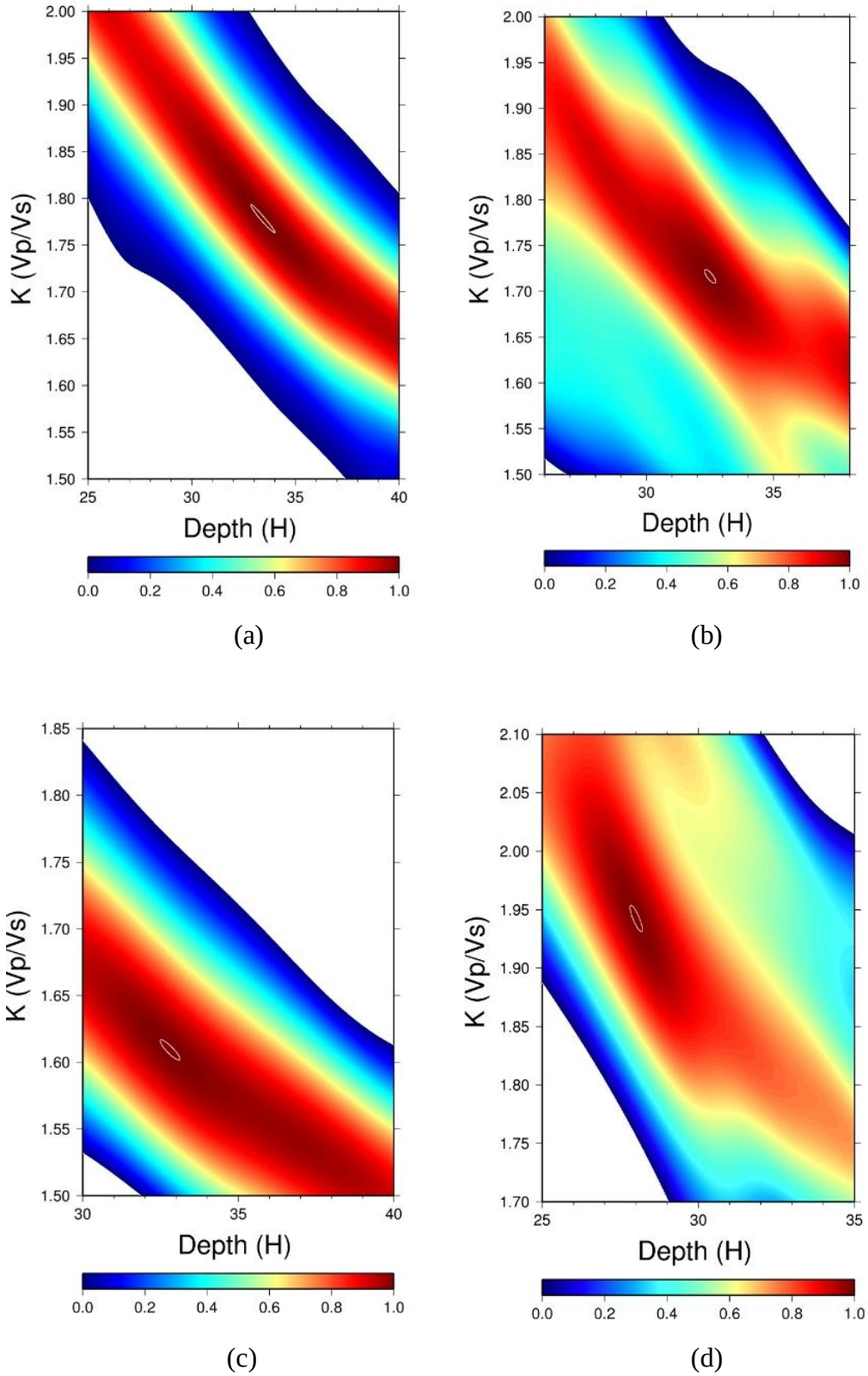

Figure 4.7. H-κ stacking result maps for stations a) CTYL , b) EDC , c) ELBA and d) ENEZ.

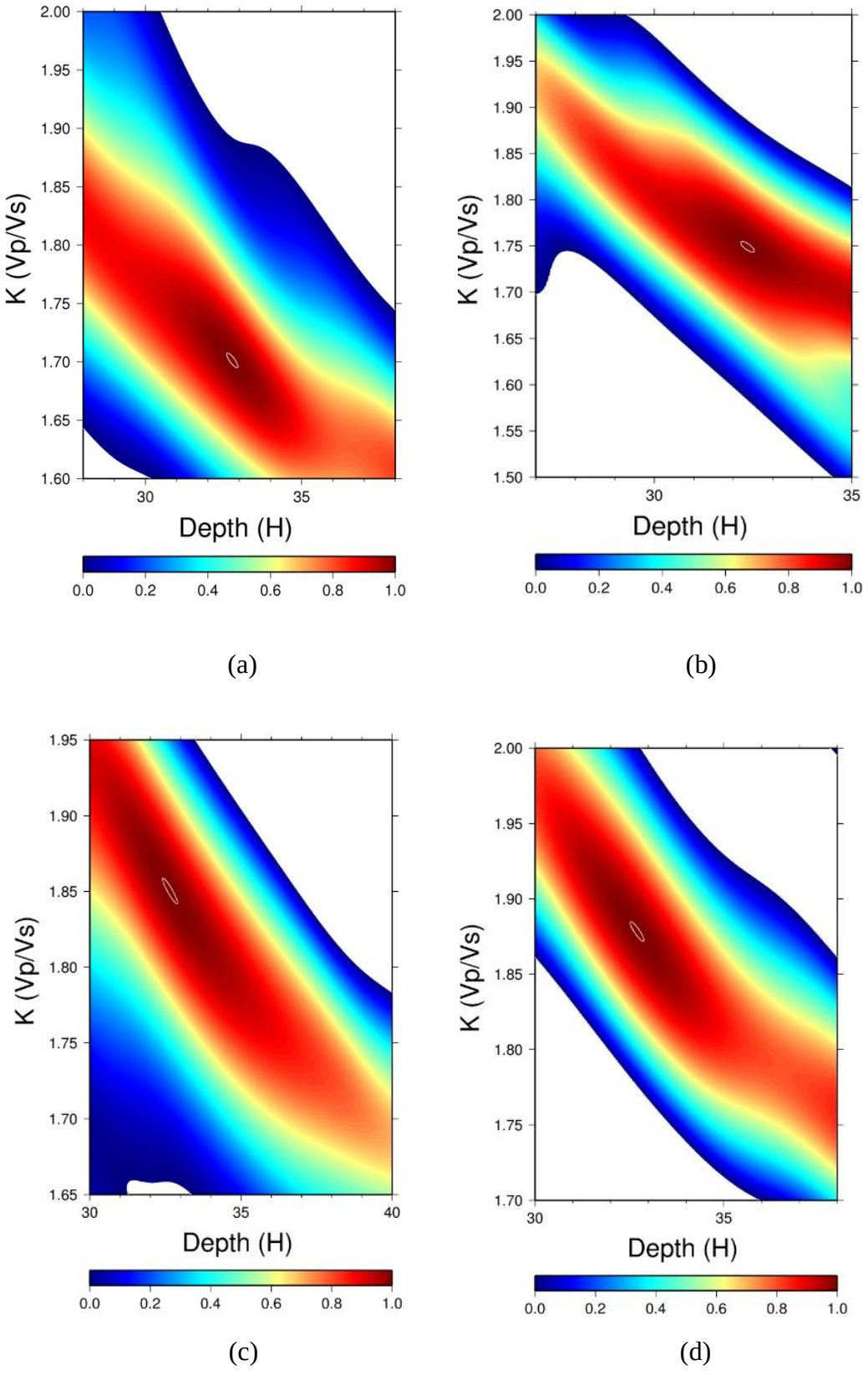

Figure 4.8. H-κ stacking result maps for stations a)ERIK, b) ESKM, c) GADA and d) GELI.

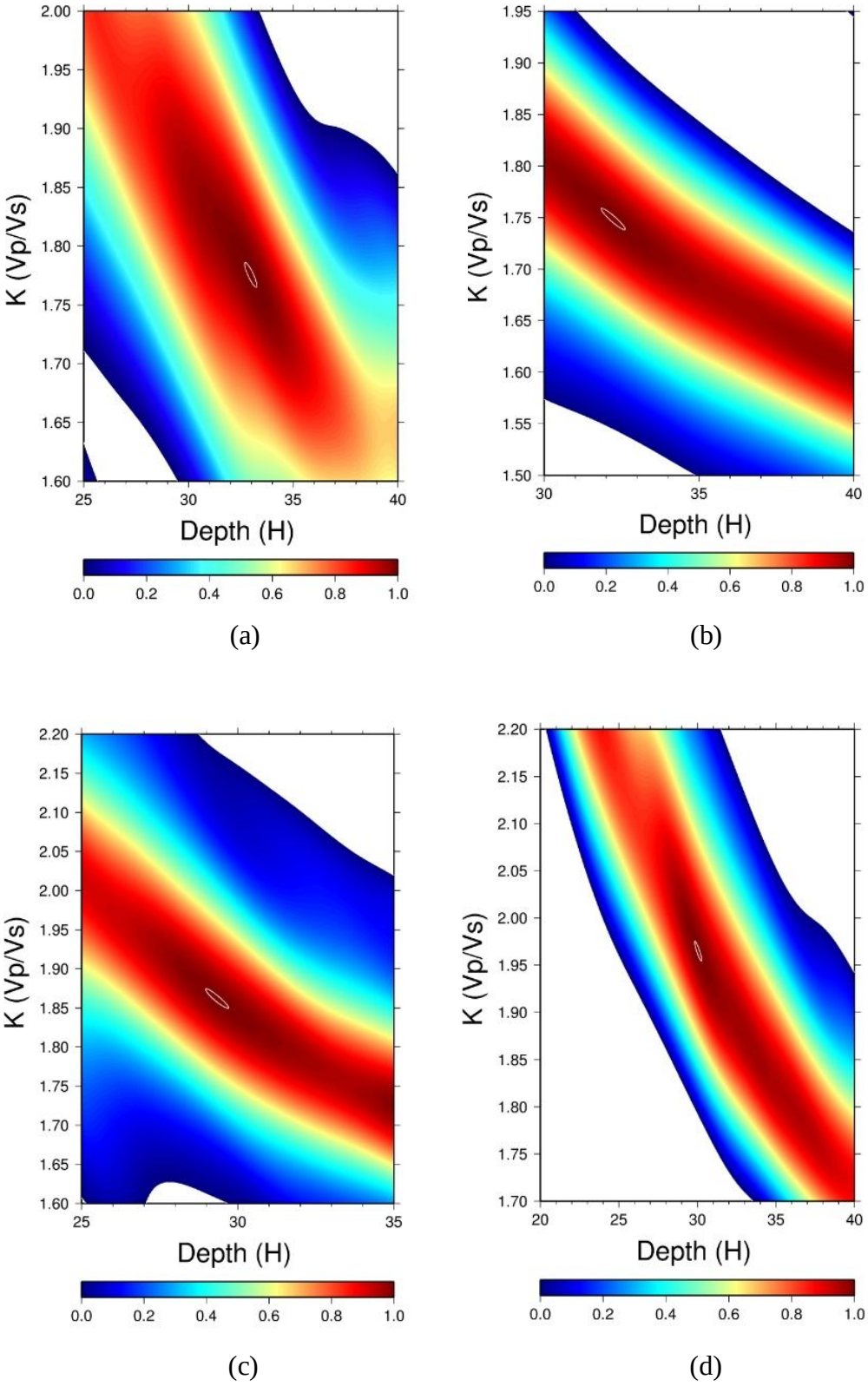

Figure 4.9. H-κ stacking result maps for stations a) GEMT, b) IGDM, c) ISK and d) KLYT.

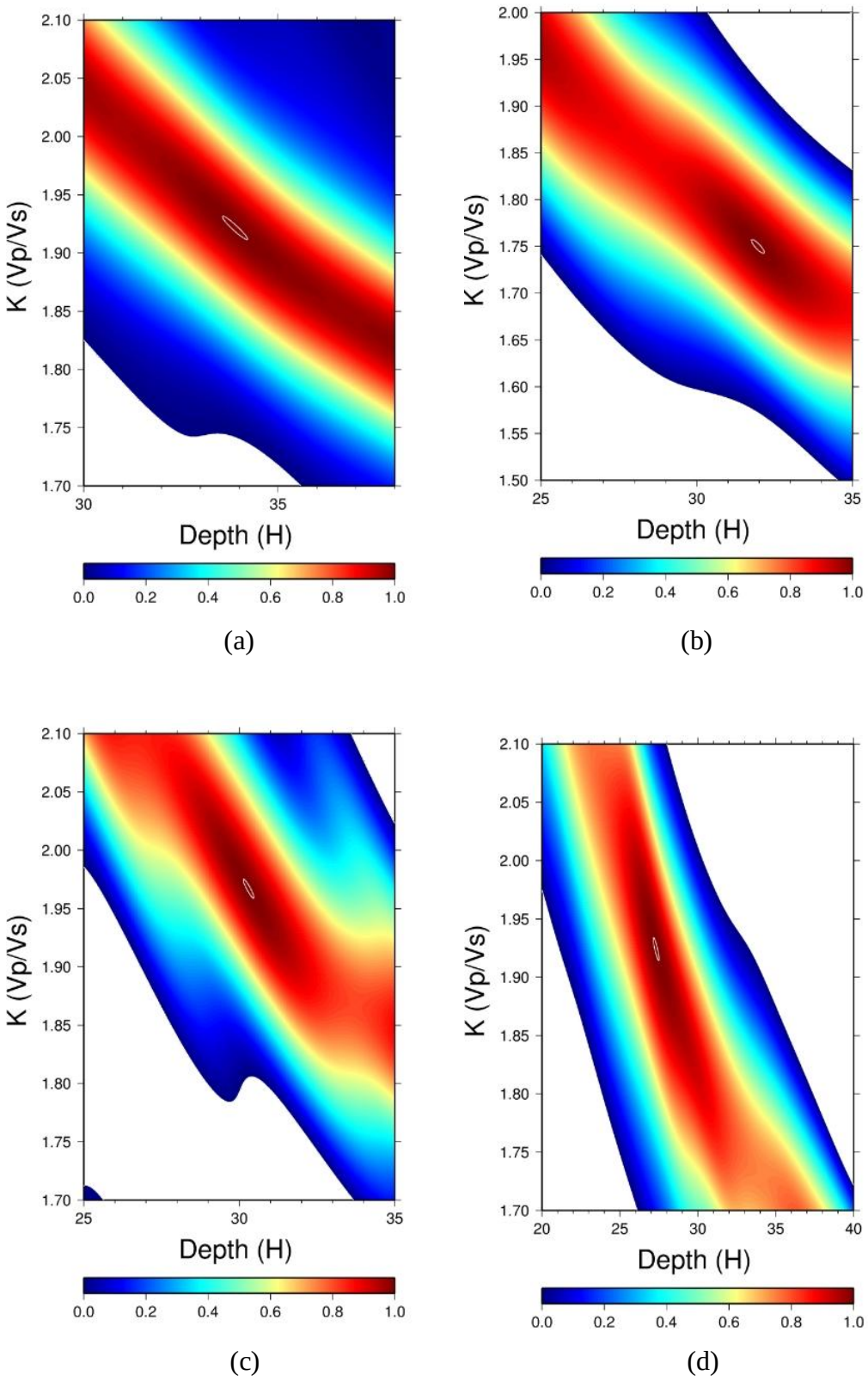

Figure 4.10. H-κ stacking result maps for stations a)KMRM, b) KNLM, c) LAP and d) MARM.

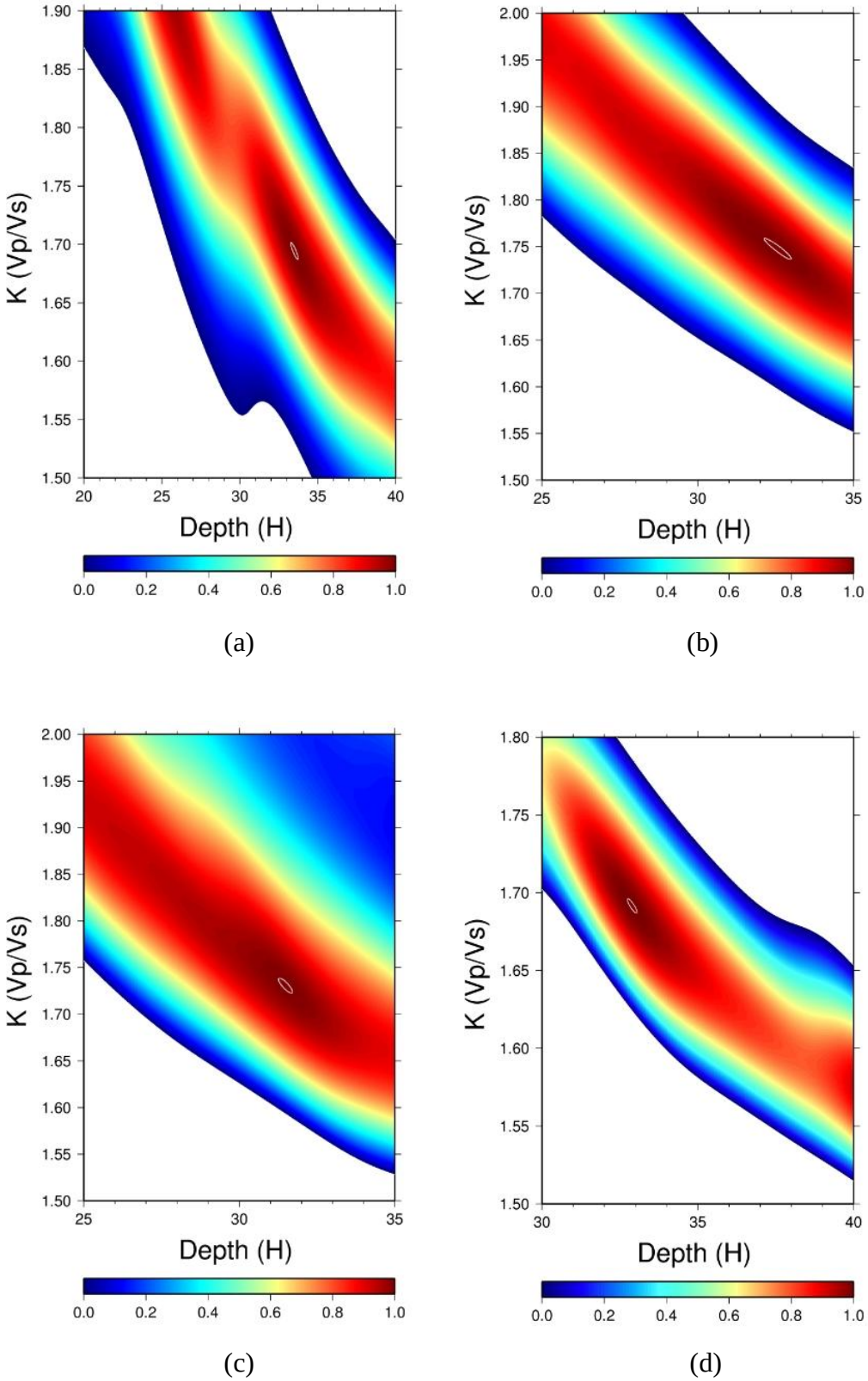

Figure 4.11. H-κ stacking result maps for stations a)MDNY, b) MYCM , c) NEVM and d) SBT1.

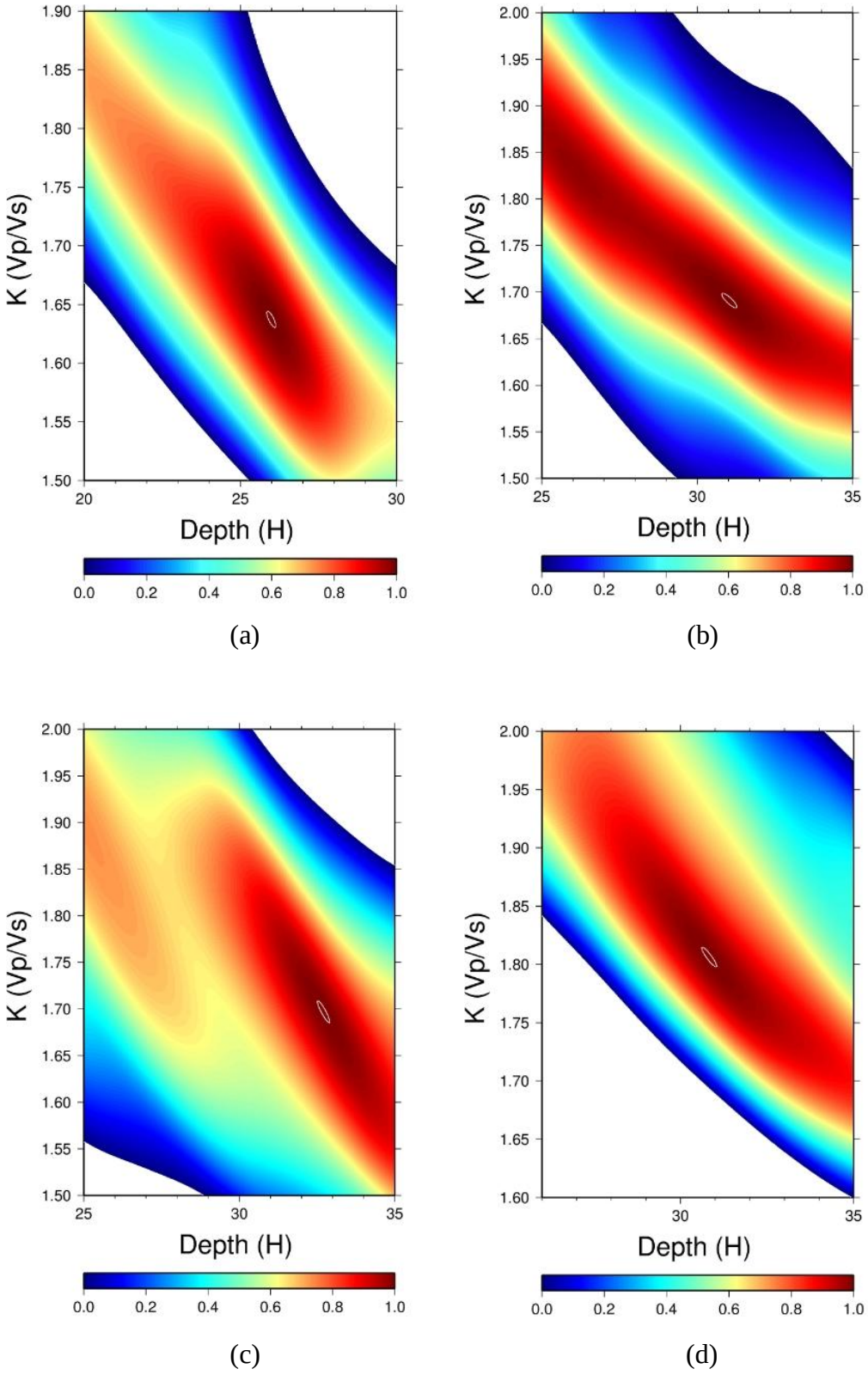

Figure 4.12. H-κ stacking result maps for stations a) SBT4, b) SBT5, c) SGTM and d) SLVM.

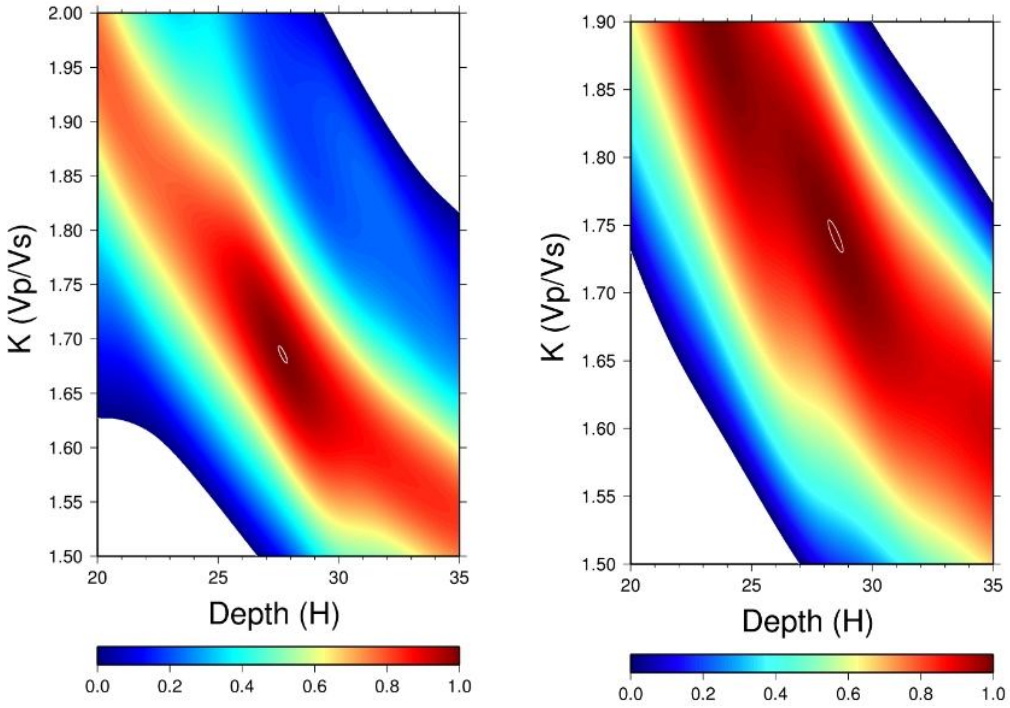

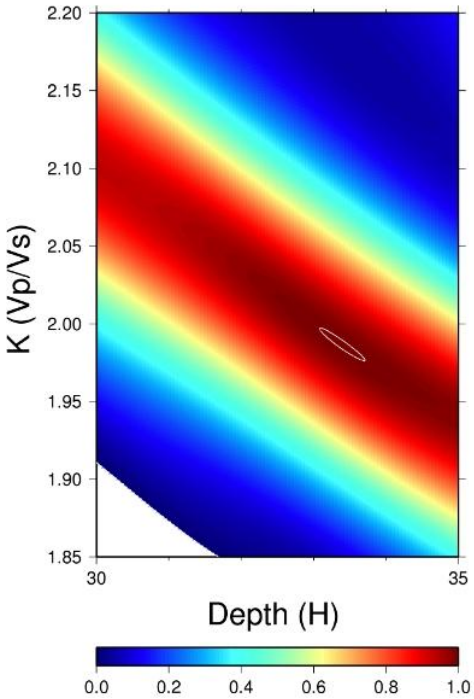

Figure 4.13. H-κ stacking result maps for stations a) TRNM, b) KCTX and c) MFTX.

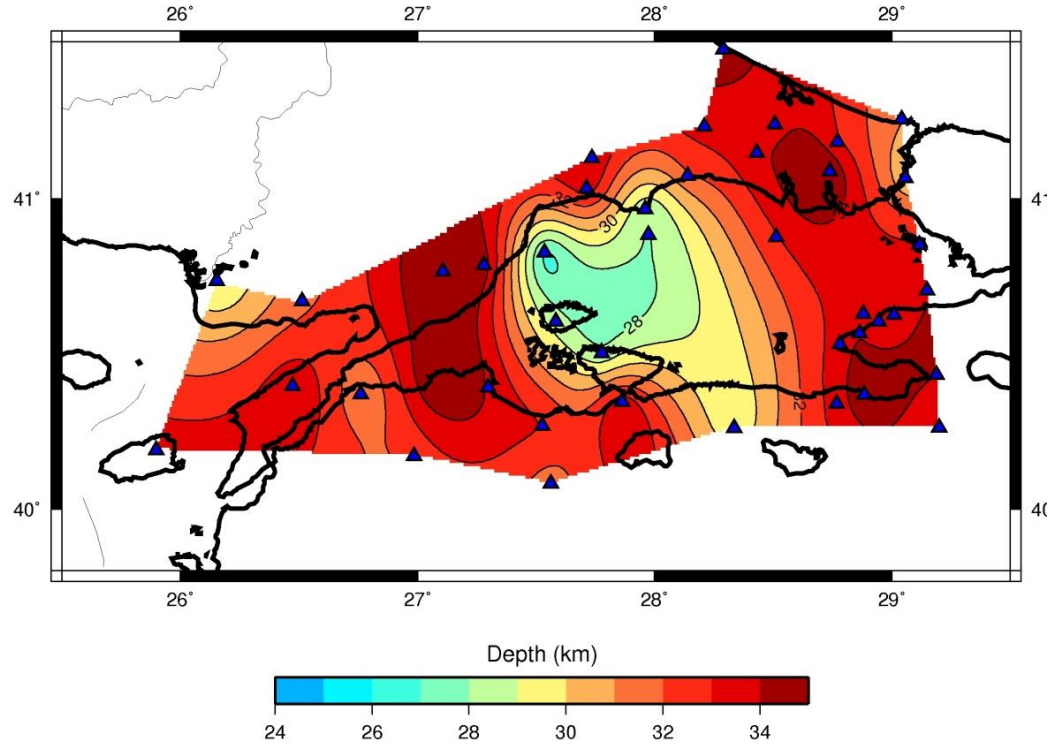

Figure 4.14. The final Moho depth map.

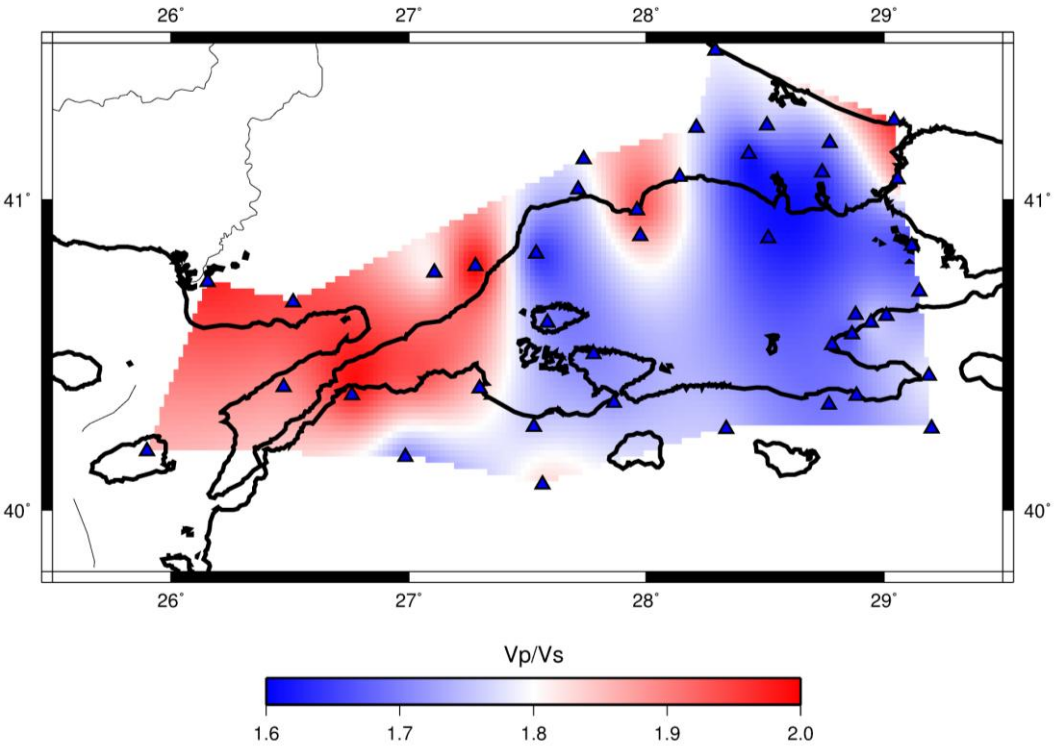

Figure 4.15. The final Vp/Vs ratio map.

4.3. Results of Linearized Iterative Inversion Method

Additionally, we applied 1D linearized iterative inversion method suggested by Ammon (1991) to KCTX station in order to define Moho depth and observe velocity variation of the layers. First of all, we stacked the radial receiver functions coming from the same direction. Furthermore, we stacked the RFs and plotted the high, low, and average amplitude evalues as it was given in Figure 4.15.

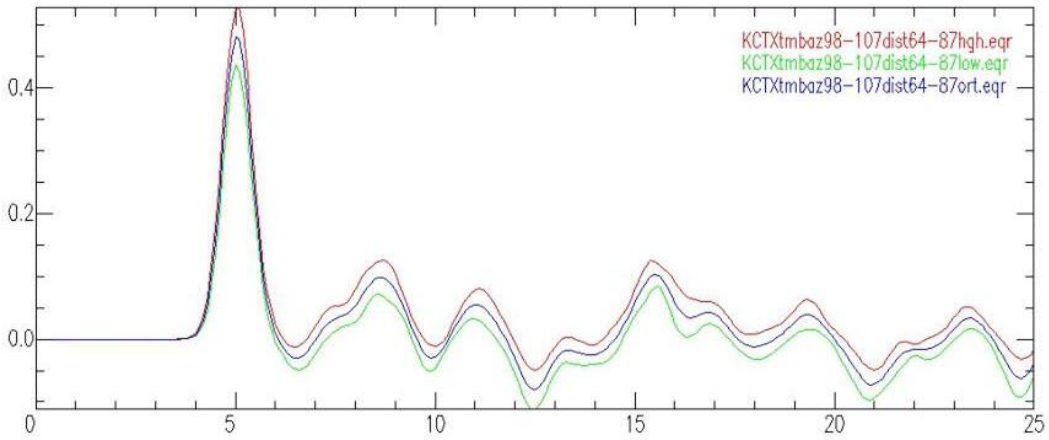

Figure 4.16. The high, low, and average amplitudes obtained from the RFs.

After the stacking of RFs, an initial velocity model was choosen (Gürbüz *et al.*, 2000) and single inversion was applied to the stacked RFs (Figure 4.16).

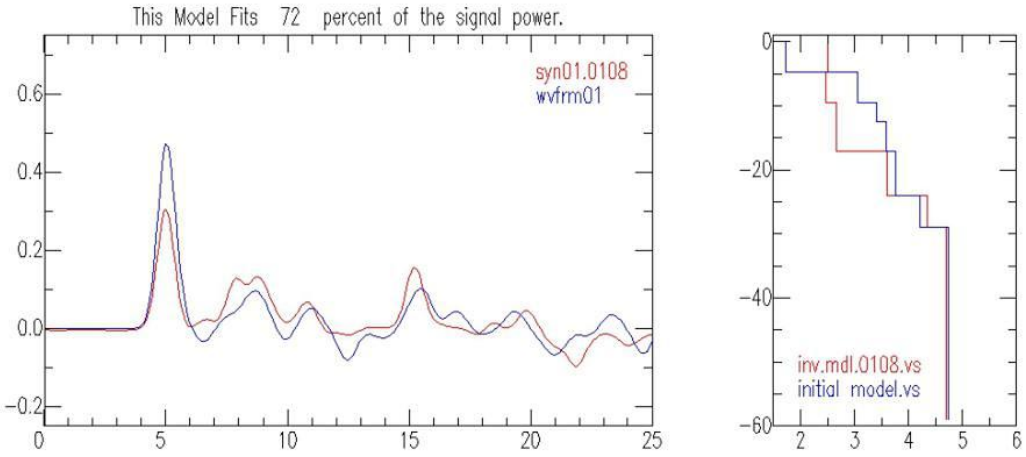

Figure 4.17. Single inversion by using the velocity model of Gürbüz *et al.*, (2000).

In the next step, we changed the initial model and increased the layer number to determine the velocity varition. After, weapplied the single inversion again we found a new synthetic receiver function (Figure 4.17).

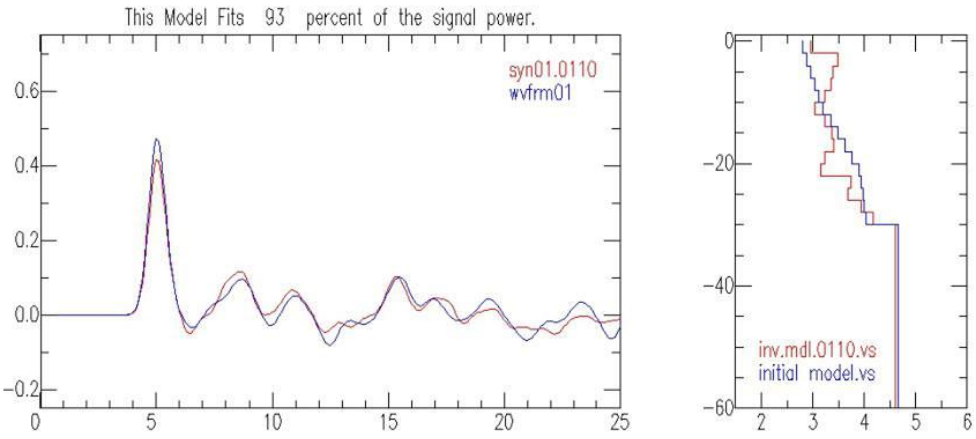

Figure 4.18. Single inversion by using the modified velocity model.

According to this 1D inversion method, we can clearly see the velocity perturbations of layers. The inversion result from receiver functions depends on the initial model, because receiver functions are sensitive only to the relative information of the velocity structure. Therefore, this method requires an initial model as close as possible to the true crustal model. Hence, we used the velocity model of Gürbüz *et al.*, (2000) as initial model which gives an average velocity model for the Marmara region covering the area where KCTX station is installed. After that, we realized that model fits the observations relatively well by increasing the number of layers and changing the Vp and Vs values. For KCTX station, the model fit increased from 72 % to 93 % after the inversion steps which are mentioned above. On the other hand, if we compare the results of H-κ stacking method with the 1D inversion method suggested by Ammon (1991) it can be clearly seen that the Moho depth is similar to one another, 28 km and 30 km respectively.

5. CONCLUSION AND DISCUSSIONS

Receiver functions of teleseismic events from permanent land and sea bottom seismic stations have been analyzed to determine the variation of the thickness of the crust and Vp/Vs ratios in the Marmara Region.

According to our result, ISK, KLYT and ALTM stations which are located in the northern part of the Marmara Region, Moho depth is between 29-30 km and Vp/Vs ratio is between 1.81-1.96. Zor (2006) found a similar Moho depth of 32 km for the ISK station from a recever function study. Gürbüz *et al.,* (1991) estimated the thickness of the crust of ISK station as 26 km from a study which is related to crustal structure using earthquake travel time data. In the western part of these two stations, the Moho depth is between 32–33 km for BGKT, CTKS, ELBA, and CTYL stations. Vp/Vs ratios of 1.70-1.78 for BGKT, CTKS, CTYL and 1.60 for the station ELBA are relatively low with respect to the values obtained for the station mentioned above. Unlike ELBA, the others are close to normal Vp/Vs ratios (1.73), which were installed on or close to very old geologic units.

In the eastern part of the area, Moho depth changes from approximately 30 to 32 km for BUYM, SBT1, SBT5, ESKM, ARMT, BOZM, GEMT stations which are located near Çınarcık Basin. Zor (2006) found that the thickness of the crust is 30 km for BOZ station. Moreover, Vp/Vs ratio is between 1.74-1.77 for ESKM and GEMT stations and 1.64-1.69 for the other stations which are mentioned above, respectively. These low values can be related to basin type structures in the area and also these stations were installed on the geothermal area with fluid filled cracks.

In the southern part of the region, the Moho depth is nearly between 28-32 km and Vp/Vs ratio changes between 1.71-1.81 for the IGDM, KCTX, EDC, KNLM, ATIM, BZGM stations. For KCTX station 1D velocity inversion method was applied and Moho depth was found as 30 km which is similar results obtained by H-κ stacking method.

In the western part of the region we observed that high Vp/Vs ratios which 1.85–1.96 for the GELI, LAP, GADA, ENEZ and ERIK stations. The Vp/Vs ratio is relatively

high with respect to the other areas. Probably, Vp is higher in this area because of the metamorphic grade and increasing mafic content in the same region. On the other hand, crustal thickness in that region was found approximately 28–32 km.

Surrounding the North Marmara Trough, Moho depth is shallower than the other areas because of the extentional basin structure. We observed that Moho depth is between 26-28 km in that region. Especially MARM, SBT4, and TRNM stations have shallower structure. In that region our results are similar to results of Bécel *et al*., (2000) which suggested a shallower Moho depth with respect to the western and eastern land areas in the Marmara Region. Furthermore crustal thinning is also consistent with the tectonic features and the tectonic evolution of the region between Northern Boundary Normal Fault and Southern Boundary Normal Fault according to Ateş *et al.,* (2003).

In conclusion, the crustal thickness of the crust and Vp/Vs ratios vary in Marmara Region because of the tectonics of the region and existence of basin structure and sedimentary layers. Vp/Vs ratio is highly affected by the composition of the upper crust that vary from sandstone to limestone. And also thickness of the lower crust affects the Vp/Vs ratio and causes to increase there. In general, lower crust consists of mafic rock having high Vp/Vs ratio. So, low Vp/Vs ratios can be related to decreasing crustal thickness which means thinning lower crust and change in the composition of the upper crust.

In our study, we found that the average Moho depth and average Vp / Vs ratio is 31 km and 1.74 respectively. Average Moho depth in our result matches well with the previous studies such as Horasan *et al.,* (2002), Zor *et al.,* (2006), Mutlu (2011) and Vanacore *et al.,* (2013). In future studies, we will focus on 1D velocity model inversion technique for the same stations and new SBT stations to be installed in March 2014 (Turkish – Japanese Project and IFREMER – Marsite Project) in the Marmara Region to determine S wave velocity structure and investigate anisotropy and dipping of the Moho by examining earthquakes coming from different backazimuths.

REFERENCES

Altıner, D., A.Koçyiğit, A.Farinacci, U. Nicosia, M.A. Conti, 1991, "Jurassic, Lower Cretaceous Stratigraphy and Paleogeographic Evolution of the Southern Part of North Western Anatolia", *Geologica Romana,* 28, 13-80.

Ammon, C.J., G.E. Randall, and G. Zandt, 1990, "On the Nonuniqueness of Receiver Function Inversions", *J. Geophys Res*., 95, 15, 303-15, 318.

Ammon, C.J., 1991, "The Isolation of Receiver Effects from Teleseismic P Waveforms", *Bull. Seismo. Soc. Am*., 81, 2504-2510.

Aydın, Y., 1974, *Etude Pétrographique et Géochimique de la Parte Centrale du Massif d'Istranca (Turquie),* PhD Thesis, Université de Nancy, 131.

Barış, Ş., J. Nakajima, A. Hasegawa, Y. Honkura, A. Ito, and B. Üçer, 2005, "Three-Dimensional Structure of Vp, Vs and Vp/Vs in the Upper Crust of the Marmara Region, NW Turkey", *Earth Planets Space*, Vol. 57, 1019-1038.

Bayrakçı, G., 2009, *Hétérogénéité 3D de la Croûte Supérieure Sous la Mer de Marmara: Tomographie sur une Grille de Sismomètres Fond de Mer et de Profils de tirs*, Ph. D. Thesis, Institut de Physique du Globe de Paris Université Denis Diderot.

Bécel, A., 2006, *Structure Sismique de la Faille Nord Anatolienne en Mer de Marmara*, Ph.D. Thesis, Institut de Physique du Globe de Paris.

Bécel, A., M. Laigle, B. de Voogd, A. Hirn, T. Taymaz, A. Galvé, H. Shimamura, Y. Murai, J. Lépine, M. Sapin, & S. Özalaybey, 2009, "Moho, Crustal Architecture and Deep Deformation under the North Marmara Trough, from the Seismarmara Leg1 Offshore-Onshore Reflection-Refraction Survey". *Tectonophysics* Vol. 467, 1–21.

Bécel, A., M. Laigle, B. Voogd, A. Hirn, T. Taymaz, S. Yolsal-Çevikbilen, H. Shimamura, 2010, "North Marmara Trough Architecture of Basin Infill, Basement and Faults, from PSDM Reflection and OBS Refraction Seismics", *Tectonophysics*, Vol. 490, 1–14, DOI:10.1016/j.tecto.2010.04.004.

Burdick, L.J., and Langston, C.A., 1977, "Modelling Crustal Structure Through the Use of Converted Phases in Teleseismic Body-Waveforms", *Bull. Seismo. Soc. Am.* 67, 677-691.

Cassidy, J.F., 1992, "Numerical Experiments in Broadband Receiver Function Analysis", *Bull., Seismo. Soc. Am.*, 82, 1453-1474.

Dean, W.T., F. Martin, O. Monod, O. Demir, R. B. Rickards, P. Bultynck, N. Bozdoğan, 1997, "Lower Paleozoic Stratigraphy, Karadere–Zirze Area, Central Pontides Northern Turkey. In: Lower Palaeozoic Evolution in Northwest Gondwanaland Göncüoğlu, M.C., Derman, A.S. (Eds.)", *Turkish Association of Petroleum Geologists,* Vol. 3, 32–38 (special publications).

Denli, A., 2008, *3-D Velocity Structure of Eastern Marmara Region from Local Earthquake Tomography*, M.Sc. Thesis, KOERI.

Dey-Sarkar, S.K. and Wiggins, R.A., 1976, "Source Deconvolution of Teleseismic P Wave Arrivals between 14-40 Degrees", *J. Geophys.Res*. 81, 3633-3641.

Görür, N., M. N. Çağatay, M. Sakınç, M. Sümengen, K. Şentürk, C. Yaltrak, A. Tchapalyga, 1997, "Origin of the Sea of Marmara as Deducted from the Neogene to Quaternary Paleogeographic Evolution of its Frame", *International Geology Review,* Vol. 39, 342–352.

Gürbüz, C., S. Püskülcü., S. B. Üçer., 1991, "A Study of Crustal Structure in the Marmara Region Using Earthquake Data". Multidisciplinary Research on Fault Activity in the Western Part of the North Anatolian Fault Zone (4).

Gürbüz, C., M. Aktar, M., H. Eyidoğan, A. Cisternas, H. Haessler, A. Barka, M. Ergin, N. Türkelli, O. Polat, B. Üçer, S. Kuleli, Ş. Barış, B. Kaypak, T. Bekler, E. Zor, F. Biçmen, A. Yörük, 2000, "The Seismotectonics of the Marmara Region (Turkey): Results from a Microseismic Experiment", *Tectonophysics*, Vol. 316, 1-17.

Helmberger, D. V., and Wiggins, R., 1971, "Upper Mantle Structure of Midwestern United States", *J. Geophys.Res*. 76, 3229-3245.

Horasan, G., L. Gülen, A. Pınar, D. Kalafat, N. Özel, H.S. Kuleli and A.M. Işıkara, 2002, "Lithospheric Structure of the Marmara and Aegean Regions, Western Turkey", *Bull. Seismo. Soc. Am*., V92(1) 322 – 329.

Işık, S. E., 2013, *3-D P Wave Velocity Structure of Marmara Region Using Local Earthquake Tomography*, M.Sc. Thesis, KOERI.

Julia, J., and J. Mejia, 2004, "Thickness and Vp/Vs Ratio Variation in the Iberian Crust", *Geophys. J. Int.*, 156, 59-72.

Julia J., F. Mancilla and J. Morales, 2005, "Seismic Signature of Intracrustal Magmatic Intrusions in the Eastern Betics (Internal Zone), SE Iberia", *Geophys. Res. Lett.*, 32, L16304 doi:10.1029/2005GL023274.

Karabulut, H., S. Özalaybey, T. Taymaz, M. Aktar, O. Selvi, A. Kocaoğlu, 2003, "A Tomographic Image of the Shallow Crustal Structure in the Eastern Marmara", *Geophys. Res. Lett.*, Vol. 30, 10-1–10-4.

Kikuchi, M. and H. Kanamori, 1982, "Inversion of Complex Body Waves", *Bull. Seismo. Soc. Am.*, 72, 491-506.

Langston, C.A., 1979, "Structure under Mount Rainier, Washington, Inferred from Teleseismic Body Waves", *J. Geophys. Res.*, 84, 4749-4762.

Liggoria, J.P., and C.J. Ammon, 1999, "Iterative Deconvolution and Receiver Function Estimation", *Bull. Seismo. Soc. Am*., 89, 1395-1400.

Liggoria, J.P., 2000, *The Mantle-Crust Transition Beneath North America*, Ph.D. Thesis, Deparment of Earth Atmospheric Sciences St. Louis University.

McKenzie, D., 1972, "Active Tectonics of the Mediterranean Region", *Geophys. J. Roy. Ast. Soc*. 30, 109-185.

Moore, W.J., E.H. McKee, Ö. Akıncı, 1980, "Chemistry and Chronology of Plutonic Rocks in the Pontid Mountains, Northern Turkey", *European Copper Deposits*, Vol. 1, 209–216.

Kömeç Mutlu A., H. Karabulut, 2011, "Anisotropic Pn Travel Time Tomography of Turkey and Adjacent Regions", *Geophy. J. Int.,Vol.* 187, Is 3, pp 1743-1758.

Okay, A.I., O. Tüysüz, 1999, "Tethyan Sutures of Northern Turkey. In: Durand, B., Jolivet, L., Horváth, F., Séranne, M. (Eds.), The Mediterranean Basins: Tertiary Extension within the Alpine Orogen", *Geological Society, London*, 475–515 (special publications).

Okay, A., 2008, "Geology of Turkey", A synopsis. *Anschnitt*, Vol. 21,19–42.

Owens, T.J., Zandt, G., and Taylor, S.R., 1984, "Seismic Evidence or an Ancient Rift Beneath the Cumberland Plateau, Tennessee: A Detailed Analysis of Broadband Teleseismic P Waveforms", *J. Geophys.Res.* 89, 7783-7795.

Özalaybey S., Savage M.K., Sheehan A.F., Louie J.N., Brune J.N., 1997, "Shear-wave Velocity Structure in the Northern Basin and Range Province from the Combined Analysis of Receiver Function and Surface Waves", *Bull. Seismo. Soc. Am.*, 87, 183–199.

Phinney, R. A., 1964, "Structure of Earth Crust from Spectral Behavior of Long-period Waves", *J. Geophys. Res*., 69, 2997-3017.

Randall, G. E., 1989, "Efficient Calculation of Differential Seismograms for Lithospheric Receiver Functions", *Geophys. J. Int*., 99, 469-481.

Scherbaum, F. and Johnson J., 1992, "PITSA, Programmable Interactive Toolbox for Seismological Analysis, IASPEI Software Library, Editor Lee W.H.K., Vol.

Vinnik, L.P. and Kosarev, G.L., 1981, "Determination of Crustal Parameters from Observations of Teleseismic Body Waves". Proc. Acad. Sci. USSR, 261, 1091-1095.

Tüysüz, O., 1993, "Karadeniz'den Orta Anadolu'ya bir Jeotravers: Kuzey Neo-Tetis'in Tektonik Evrimi", *Türkiye Petrol Jeologları Derneği Bülteni*, 5, 1–33.

Zattin, M., Okay, A.I. & Cavazza, W., 2005, "Fission-track Evidence for Late Oligocene and Mid-Miocene Activity along the North Anatolian Fault in South-western Thrace". *TerraNova*, 17, 95-101.

Zattin, M., W. Cavazza, A. I. Okay A, I. Federici, M. G. Fellin, A. Pignalosa, P. Reiners, 2010, "A Precursor of the North Anatolian Fault in the Marmara Sea Region", *Journal of Asian Earth Sciences*, Vol. 39, pp. 97–108

Zelt, B.C. and Ellis, R.M., 1998, "Receiver Function Studies in the Trans-Hudson Orogeny, Saskatchewan", *Can.J.Earth. Sci.*, 36, 585-603.

Zhu, H. and Kanamori, H., 2000, "Moho Depth Variation in Southern California from Teleseismic Receiver Functions", *J. Geophys.Res.* 105, 2969-2980.

Zor, E., 2002, *The Shear Wave Velocity Structure of the Eastern Marmara Region by Using Receiver Function Analysis*, Ph.D. Thesis, *Boğaziçi Univ. Library*, Turkey.

Zor, E., S. Özalaybey, C. Gürbüz, 2006, "The Crustal Structure of the Eastern Marmara Region, Turkey by Teleseismic Receiver Functions", *Geophysical Journal International*, Vol. 167, 213-222.